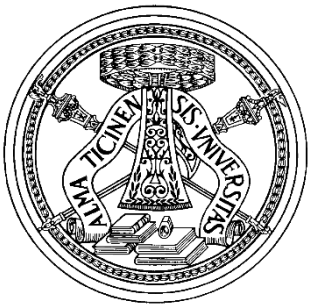

Università degli Studi di Pavia

Dottorato di Ricerca in
Ingegneria Elettronica, Informatica ed Elettrica
Ciclo XXIX

Non-invasive and contact-less detection of the cardiovascular system status

Antonio Mariano

Year 2016

Contents

List of figures III

List of tables V

Introduction VII

1. Cardiovascular Diseases (CVD): a brief review 1

   a. Diseases and their causes 1

      i. Cardiovascular Diseases Description 1

      ii. Risk factors 3

   b. Incidence 5

      i. Epidemiology 5

      ii. Economic burden 6

2. Background on Biophotonics for Cardiovascular Application 9

   a. Photonics for cardiovascular surgery 9

      i. Myocardial Laser Revascularization (MLR) 9

      ii. Laser-assisted vascular welding (LAVW) 13

   b. Photonics for Intravascular imaging and sensing 16

      i. Intravascular Optical Coherence Tomography (IVOCT) 16

      ii. Catheter-based Near Infrared Spectroscopy (NIRS) 20

      iii. Optical fiber pressure sensor (OFPS) 22

   c. Background knowledge 27

      i. Pulse Wave Velocity and Arterial Stiffness 27

      ii. Laser Triangulation 30

d. Advantages 31

i. Light technologies 31

ii. Nistas project 32

3. NISTAS Project 34

a. Prototypes Architecture and workflow 35

iii. Prototype 1 35

iv. Prototype 2 37

iii. Procedure 40

b. Algorithm 41

c. Final Results 47

v. Prototype 1 47

vi. Prototype 2 52

4. Conclusions 53

Bibliography 56

List of figures

Figure 1-1: Age-standardized deaths due to cardiovascular disease (rate per 100,000) 5

Figure 1-2 CVD risks in relation to national income. Results for (A) males and (B) females. 6

Figure 2-1 Trans Myocardial Laser Revascularization with CO2 laser [28] 11

Figure 2-2 Trans Myocardial (a) and Percutaneous Myocardial (b) laser revascularization with Ho:Yag laser [30] 12

Figure 2-3 Cross-sectional OCT image of healthy segment of coronary vessel presenting the internal elastic lamina (IEL), the media (M), external elastic lamina (EEL) and adventitia (AD) [40] 18

Figure 2-4 (B) Cross-sectional OCT image of fibrotic lesions. (C) Cross-sectional OCT image of lipid-rich lesion covered with thin fibrous cap atheroma (TCFA – white arrows). The image also presents small red thrombi. (D) Cross-sectional OCT image of calcification (white arrow) [40] 19

Figure 2-5 Near-infrared spectra of various pure substances possibly related [41] 20

Figure 2-6 two-dimensional map of the artery that indicates the location of lipid core plaque [43] 21

Figure 2-7 OCT-NIRS images of cadaver coronary artery ex vivo. OCT images show lesions with reduced backscattering. NIRS image shows absorption spectra of tissue versus wavelength, representing the total attenuation normalized for the entire data set; 22

Figure 2-8 Examples of numerical aperture overlapping. (A) Target near to the fibers; (B) Target far from the fibers; (C) Diagram of the intensity vs the displacement of the target [46]. 24

Figure 2-9 Fiber strain and wavelength shift 25

Figure 2-10 - Schematic of pressure transducer based on Fabry-Perot [49] 26

Figure 3-1 - Reference triangle 30

Figure 3-2 Laser triangulation system [60] 31

Figure 3-3 Keyence LJV-7080 head 36

Figure 3-4 Complete system 37
Figure 3-5 Mechanical scheme of the optical module.....38
Figure 3-6 Directions of the projected light lines and of observations from the camera. 39
Figure 3-7 Graphical representation of an acquisition matrix. (Z) is the height in A.U., (x) the number of samples of the width and (Y) the number of time samples 42
Figure 3-8 Graphical representation of the smoothing process. (Z) is the height in A.U., (x) the number of samples of the width and (Y) the number of time samples 43
Figure 3-9 Spectral coherence 44
Figure 3-10 Peaks on the heartbeat waveforms.....45
Figure 3-11 Second derivative of the original waveforms and systolic feet in reference of the pulse peaks.....45
Figure 3-12 GUI panel 47
Figure 3-13 Graphics of PWV distribution for each volunteer (upper graphic refer to left side of the neck and lower graphic refer to the right side).....49
Figure 3-14 Resampling graph 50
Figure 3-15 Re-quantization graph 51
Figure 3-16 GUI interface of Prototype 2 (data on the left are just for the sake of an example) 52
Figure 4-1 General schematic of a Mach-Zehnder homodyne interferometer (BS = beam splitter; PD = photodiode) ..... **Error! Bookmark not defined.**
Figure 4-2 General schematic of a Mach-Zehnder heterodyne interferometer (BS = beam splitter; PD = photodiode; OFS = Optical Frequency Shifter) ..... **Error! Bookmark not defined.**
Figure 4-3 interference pattern ..... **Error! Bookmark not defined.**
Figure 4-4 Self-mixing with a diode laser [64] ..... **Error! Bookmark not defined.**
Figure 4-5 – Self-mixing signal [64] s..... **Error! Bookmark not defined.**
Figure 4-6 schematics of a heterodyne LDV [75] ..... **Error! Bookmark not defined.**
Figure 4-7 IQ Lissajous curve [75] ..... **Error! Bookmark not defined.**

List of tables

Table 1-1 Global costs attributable to CVD, and CVD incidence (in 1000s n of deaths). 7

Table 1-2 Costs attributable to CVD in 2010 by WHO sub-region 8

Table 3-1 Distribution of pulse wave velocity (m/s) according to the age category in the normal values population (1455 subjects) 29

Table 3-2 Final data acquired from ten volunteers 48

Table 3-3 Resampling table.....50

Table 3-4 Re-quantization table.....51

Table 4-1 Summary of differences between devices..... **Error! Bookmark not defined.**

Introduction

Biophotonics is a scientific sector which includes all the light-based technologies applied to life science and medicine. Many different fields of application are included in this category, each of them characterized by the kind of technology, principle or purpose.

As the name suggests, Biophotonics is a branch of a higher and wider field called Photonics which groups all those areas that manipulate “photons”, the small elementary particles composing light. The properties of photons enable a wide range of applications in Biophotonics, going from micro to macro scale. They could be used for applications going from the detection, manipulation and analysis of macromolecules, cells, subcellular structures, and tissues, to the diagnosis of medical parameters.

One of the most important properties that allowed light-based technologies to be widely used in medical field is the fact that photons are contactless, meaning that there’s no physical interaction between the instrument and the target and thus making each measurement or manipulation non-destructive and allowing for the preservation of the biological tissues

In the broad range of fields that find a place in this discipline, some of the most important could be mentioned for the impact that they had in everyday life.

We can start by mentioning the fundamental biomedical research, which aims at understanding biological processes at cellular or molecular level that is the very starting point for the comprehension of the genesis of diseases. Furthermore, light technology helps also the pharmaceutical research to establish how drugs impact on such diseases. These technologies are also useful in laboratory test or point of care diagnosis, as they are employed in the analysis of body liquids, and in clinical diagnosis, in which imaging finds an important role in many medical disciplines such as cardiology, ophthalmology, and oncology.

There are also other applications that have an indirect impact on the health of the biological tissues, which can find support from the light technologies. For example, these are used for environmental control and food safety to find potentially harmful compounds or pathogens, and for security application as detection of dangerous biological and chemical substances.

Biophotonics applications are mainly motivated by the impact they could have on society. In industrialized countries, the demographic changes are tending towards a society in which the ratio between elderly and working-age people is increasing year by year. This means that the typical disease of aged people will influence exponentially the expenses of the public health system, which should bear a rising number of people to care. In this perspective, Biophotonics can meet the needs for early and focused intervention that allows preventing and even to avoid diseases. This will lead to an improvement in people's lives and to a cut on therapeutic and follow-up costs.

Projection reported by World Health Organization (WHO) [1] shows indeed that, by the year 2050, the percentage of aged people beyond 65 years will grow by 70% and, knowing that main causes of death for this age range are and will be Cardiovascular Diseases, that mean that more people need specific health care.

So, as since the 70`s, imaging of the cardiovascular system by intravascular ultrasound was used as a valid guide in chirurgical interventions, more efforts were made to enhance this field. Indeed, years later, many light-based technologies were developed to obtain more precise information about vessels and the cardiovascular system in general, allowing less invasive and so shorter hospitalizations. This laid the foundation to the diffusion of the light technologies in cardiovascular medicine and, since then, photonics was used in prevention, analysis, intervention and therapy of the heart-related diseases.

This trend is the starting point of my thesis work, as it aims to the realization of a medical device useful for prevention and early diagnosis of cardiovascular pathology by employing laser-based technique.

In order to describe the background in which the result of my work is projected, the first chapter is dedicated to show which are the mains cardiovascular pathologies and their causes together with general considerations on which is their impact on society both epidemiological and economical. To the definition of this background, the second chapter contributes with the description of the current most diffused light-based technology for cardiovascular analysis and intervention first to help the reader to get familiar with the potential application of lasers in cardiovascular medicine and then to point out which are the lacks of current techniques.

Following chapter is the core of this thesis and my work. Here is described every aspect of my work in NISTAS (Non-Invasive Screening of the sTatus of the vAscular System) project, mainly based on the technical aspects and expressed in the research of efficient solutions to overcome the problems encountered in the building of the final prototype and in the definition of an algorithm to detect and analyze data. To be easier for the reader to understand theories and technologies used in my work, a brief description is provided at the beginning of the chapter. At this point, will be provided a comprehensive description of the two prototypes realized for this project, followed by the use procedure designed for this application and the description of the detection and analysis algorithm tailored on our requirements. In order to complete the presentation of this work, earlier and later analysis made in collaboration with the Centre of Genetic and Cardiovascular diseases of the “San Matteo” Hospital in Pavia are presented as an indicator of the achieved objectives and margins of improvement.

In the end, a recapitulation will give an organic view of this thesis to remark the state-of-the-art and point out the needs of the cardiovascular medicine that could be satisfied by our device.

1. Cardiovascular Diseases (CVD): a brief review

In this chapter, I will introduce which are the main disease affecting the cardiovascular system and the impact they have on the global economy. This is necessary to understand in which scenario this thesis work is settled.

a. Diseases and their causes

i. Cardiovascular Diseases Description

Before talking about how the Biophotonics can help preventing Cardiovascular Diseases (CVD), it is useful to understand which are these diseases and their importance in society.

We first start to tell that, among the different CVD, only three of them are mostly responsible for worldwide deaths [2]. These are:

- Ischemic heart disease (IHD)
- Stroke
- Hypertensive heart disease (HHD)

The IHD is currently the first cause of death and the most relevant contributor to the disability-adjusted life years (DALYs), a measure of the years of live lost by the premature death from the life expectation. Indeed, in the period from 2000 to 2012, the years of life lost (YLLs) due to the IHD had an increment of 16% that translate to 160 million of YLLs, overtaking the former principal cause of death that was low respiratory infection [3]. IHD leading manifestations are angina pectoris and acute myocardial infarction (AMI) [4]. The first is presented as a pain in the chest lasting for 10 – 15 minutes and is caused by atherosclerosis, a partial occlusion of one or more coronary arteries, that leads to a reduced oxygen supply to the heart. The AMI instead, is a long-lasting pain in the chest and is caused by a total occlusion of major coronary arteries leading to the necrosis of the cardiac muscle. As it is clear, AMI is a dangerous condition that leads to a high thirty-days mortality that goes from the 3% in hospitals with advanced coronary

care unit to around 27% in hospitals with poor medical service [5]. In total, in 2012 about 7.4 million of deaths for IHD were reported worldwide placing this disease as the leading cause of death [6].

Also, the stroke [7] is a condition in which the oxygen supply is reduced, but it affects the brain. A stroke could be caused by an occlusion of the brain vessels, in which case is called ischemic stroke [8], or by a rupture of a brain vessel called hemorrhagic stroke [9]. The ischemic stroke could also be transitory [10](TIA, transient ischemic attack) which means that the occlusion of a vessel is due to a temporary blood clot and the symptoms last shortly with no damage on the brain functionality but it is, in general, an alarm for future ischemic strokes. Both ischemic and hemorrhagic strokes are instead more serious then TIA as the lack of oxygen could lead to the damage of the interested region that could end with a serious disability or with death. As mentioned, stroke is the second leading cause of death that killed about 6.7 million people only in 2012 [6].

Hypertensive heart disease (HHD) it is the third kind of CVD that, despite not being the third cause of death globally [6], it is important because shares the risk factor of IHD and strokes and can lead to them. HHD indeed, it is a direct consequence of the high pressure of the blood that causes a thickening of the blood vessel walls and so a narrowing of the vessel section [11]. This narrowing, sometimes mixed with a blood clot or cholesterol, does not allow a regular blood flow to the heart that can, therefore, be slow or can even stop. Furthermore, a heart that works under high blood pressure shows a thickening and a growth as any other muscle working under effort. This condition, called hypertrophy, change the way the heart works and consecutively the way the heart supplies blood and oxygen to the other organs.

ii. Risk factors

After Framingham Heart Studies [12] in 1948, scientists started to investigate the possible reason of CVD by monitoring people who experienced them. Results from these studies show that a huge contribution is given by an unhealthy lifestyle, which aspects can be all grouped under the Modifiable Risk Factors category, together with another category of Non-Modifiable Risk Factors that depends on predisposition to CVD [13].

In the category of Modifiable Risk Factors, we first find Hypertension that is the first leading cause of CVD [14]. It is also known as a "silent killer" as it is asymptomatic and can damage the cardiovascular system slowly and in the long term. It is usually related to other Modifiable Risk Factors from which is a direct consequence. These factors are many, and all of them can be controlled in order to have a healthy cardiovascular system. Among these, a huge role play tobacco [15] use that is responsible for 10% of the CVD worldwide [16] including passive smokers. It is a totally avoidable factor, and studies demonstrate that people who quit before 35 show a substantial reduction of coronary heart disease risk after two years, that falls to the level of non-smokers after 15 years [17]. High importance should also be given to diabetes [18] which prevalence is around 8.8 % in the world and it is responsible for 5 million of deaths, 50% of which are due to CVD [19]. The cause should be found in the high amount of glucose in the blood that it is directly proportional to the cardiovascular risk. Like any other muscle, the heart should be trained to work properly, that is why physical inactivity is a dangerous factor affecting the risk of CVD, the fourth in the world. Indeed, it is partly related to detrimental effects on blood pressure, serum lipoprotein profile (which is itself a CHD and stroke risk factor [20]) and on insulin and glucose metabolism [21]. In the end, it is unavoidable to talk about the nutrition [22]. It is well known that what we introduce in our body influence our way of living and that is true, of course, also for the influence that food has on the CVD risk. An unhealthy diet, such one with high consumption of saturated fat, trans-fat and salt lead to hypertension, high amount of

cholesterol and lipids in blood and obesity. These are all dangerous factors for the cardiovascular system as they increased the risk of strokes and others CVD.

In addition to the previously mentioned Modifiable risk factors, there is the category of Non-Modifiable Risk Factors that, as the name suggest, include those factors that we cannot control and unavoidably have weight on the insurgence of CVD. First, in the high-risk category, we find aged people. Indeed, age is the first Non-modifiable risk factor that tells us if a person is at risk of CVD, as with the advancing of age the heart undergoes physiologic changes [23]. The heart's muscles of an aged person become stiffer and stiffer, so compromising the normal function and efficiency and compounding CVD problems or their treatments. After the age, also the gender is a Non-Modifiable risk factor in the sense that men have a higher probability of encountering CVD before women. In the specific, the risk starts to increase around 10 years later for women than in men [24]. Finally yet importantly, also having a first-degree blood relative with a CHD or stroke before 55 years for male relatives or 65 for female relatives, is considered a risk factor because of genetic reason affecting the cardiovascular system [25].

Of course, if nothing can be done for this last category of risk factors, something can be done to avoid the risk of CVD by controlling or avoiding factors in the first category. Reducing, or better avoiding, tobacco use and abuse and following a healthy lifestyle, inclusive of both physical activity and a diet rich in fish, vegetables and fruit, help us to reduce the risk of CVD dramatically as much as other kinds of diseases. This can also be done as an individual choice or as a community-based intervention such as the North Karelia Project in Finland that, in the long term (1977-1995) brought to a reduction of CVD mortality by 65% nationwide [26].

b. Incidence

i. Epidemiology

The fact that we concern about Cardiovascular Diseases (CVD), as mentioned before, is because in last century they became the major cause of death and disability in the world. In particular, despite its incidence is higher in the high-income countries than in low and middle-income countries, the total amount of deaths worldwide occurs right in these countries. This could be explained by watching on Figure 1-1 that show this unbalanced distribution of death for CVD going from rates between 100 and 200 deaths per 100000 in Central Europe, Australia and United States, to high rates between 400 and 500 per 100000 in Eastern Europe, Russia, Egypt and other low and middle incomes countries. From historic trend in CHD mortality, we can also see that different regions also show different trending pattern. CHD mortality indeed, showed a rise-and-fall pattern, with a peak around 60's, in high-income countries such North and Northwestern continental Europe, United States and Australia, very different from a rising pattern characterizing the mentioned Eastern Europe and Russia [27] [28] [29] [30].

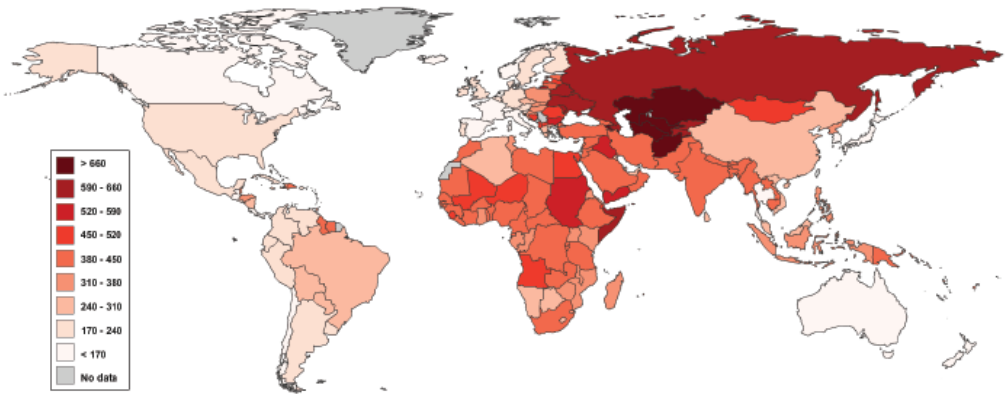

Figure 1-1: Age-standardized deaths due to cardiovascular disease (rate per 100,000)

Relying on this data, it seems that mortality rates are strictly linked to which stage of epidemiological transition a country is. The epidemiological transition is a concept proposed by Abdel Omran [31] that correlates the changes in the predominant form of disease with the

economy and health system developing of a country. For example, in an underdeveloped country, the predominant cause of death are infectious diseases but, as the economy improve, the predominant causes become non-communicable such as CVD [32]. Anyway, there seems to be a generally common pattern related to risk factors and per capita income. In Figure 1-2 [33] it is shown how the risk factors considered (Mean Body Mass Index – BMI, Mean cholesterol and systolic blood pressure (SBP)) rises as the income of a country remain low, have a peak for middle-income countries and the fall when the income gets higher.

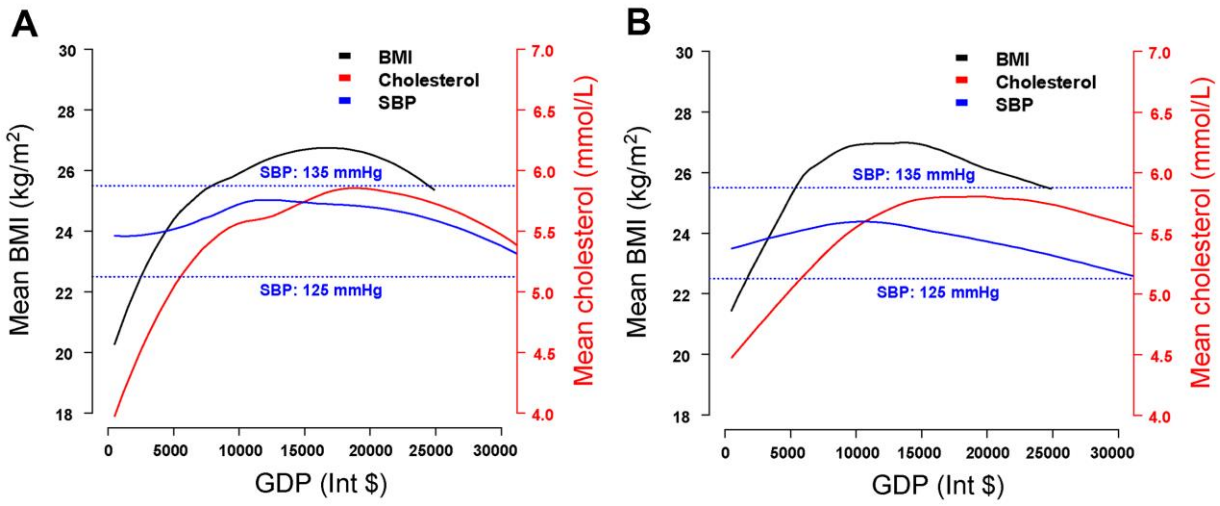

Figure 1-2 CVD risks in relation to national income. Results for (A) males and (B) females.

This reflects a complicated interaction between the stage of development of a country and its incomes. When they are low, the leading problem of a country is facing infectious disease instead of avoiding CVD risks, because of the limited resources. In addition, resources must be invested in other infrastructures that guarantee a growing economy. When a country reaches middle-income level, it means that it reaches a sustainable distribution of resources and it can face CVD problems by reversing the rising trend.

ii. Economic burden

Given the spread of CVD, we should also consider which is the economic impact that such diseases have worldwide. As already told, being the leading cause of mortality and disability, the impact on society consists not only of expenses for medical care costs such as diagnosis,

procedures, drugs and inpatient and outpatient care but also in workforce lost for a country economy. This is why the cost-of-illness (COI) is often considered to evaluate the economic burden of CV. It includes indeed the direct costs of CVD formerly mentioned and other direct costs like information, education, communication and research and income losses. Speaking of numbers, we can see from Table 1-1 based on last data available [34] [35] [36] [37] an estimation of expenses from 2010 to 2030 and the incidence due to the three main CVDs which constitute 85% of the mortality burden. Around 55% of the total cost related to CVD here showed, is due to direct cost and the other 45% to productivity loss and is so expected to increase by about 22% in 20 years.

Year	Total cost (billions of US$)	CHF incidence	IHD incidence	Stroke Incidence
2010	863	10072	24167	28299
2015	906	10821	25933	30370
2020	957	10830	28284	33122
2025	1002	12754	30369	35571
2030	1044	13637	32339	37886

Table 1-1 Global costs attributable to CVD, and CVD incidence (in 1000s n of deaths).

How these costs were distributed in 2010 can instead be seen from Table 1-2

WHO Region	Total costs (in billions of $) (without productivity costs)	Productivity costs (in billions of $)	Total Costs (in billions of $ -including productivity costs)	Per capita total costs (in $)	Per capita total costs (in $ - adults only)
AFR-D	2.9	30.	5.9	15	47
AFR-E	4.1	1.7	5.7	13	43
AMR-A	165.9	108.2	274.0	736	1206
AMR-B	8.8	17.2	26.0	52	108
AMR-D	0.9	2.1	3.1	36	91
EMR-B	4.2	7.8	12.0	70	160
EMR-D	3.5	2.9	6.3	14	41
EUR-A	197.0	90.2	287.1	627	924
EUR-B	7.5	51.1	58.6	265	501
EUR-C	7.8	39.1	46.9	194	309
SEAR-B	3.8	6.1	9.9	29	59
SEAR-D	11.3	9.5	20.8	14	32
WPR-A	36.5	26.1	62.7	372	527
WPR-B	19.8	24.7	44.4	27	48
Total	473.9	389.6	863.5		

Table 1-2 Costs attributable to CVD in 2010 by WHO sub-region – AFRO (Africa), AMRO (Americas), EMRO (Eastern Mediterranean), EURO (Europe), SEARO (South-East Asia) and WPRO (Western Pacific). The six WHO regions are further divided based on patterns of child and adult mortality in groups ranging from A (lowest) to E (highest): AFRO (D, E); AMRO (A, B, D); EMRO (B, D); EURO (A, B, C); SEARO (B, D); WPRO (A, B).

It is evident how all adds up considering that most of the costs of CVD weights on the shoulder of the high-income countries. Indeed, being the treatment and prevention of CVD a priority in this country, the total mortality is lower compared to low and middle-income countries.

2. Background on Biophotonics for Cardiovascular Application

In this chapter, I will start to describe currently most diffused optical-based technologies and how they are employed in the treatment of CVD. The aim of this chapter is to have a global view of the state-of-the-art solutions for detection and treatment of CVDs based on light technologies. The reason why I chose to illustrate both sectors is to show the tendency and so the possibility to converge in an interventional system mainly consisting in instruments based on light technologies. Advantages of this kind of technologies are robustness of the optical systems, low power consumption of fiber sensor and the possibility to reach the area where the disease is located, in a less invasive way than the traditional methods. Indeed, thanks to fiber catheters, localized ablation of a specific target can be performed by passing through the blood vessel. In the same way, fiber sensor can provide an image of the inside of the vessel in a more detailed way compared to the traditional X-ray images. I will now discuss in detail which these techniques are, how they work and the importance that they have for therapy and sensing of CVD.

a. Photonics for cardiovascular surgery

This section is dedicated to laser-based instruments used to perform localized surgery. Since their invention, lasers were used in different medicals fields as they can provide a controlled amount of energy in a specific location that can be exploited to treat diseases depending on the interaction between tissues and wavelength. Through years, many clinical studies were made to help refine fiber laser for their use in cardiovascular surgery. In the next section, some of the most important application will be described.

i. Myocardial Laser Revascularization (MLR)

We already described in the previous chapter the leading cause of death among CVD, namely IHD. In summary, this consists in an occlusion of the coronary artery that decreases the flow of

oxygen to the heart muscles (ischemia), which could bring to a heart attack and a strong pain in the chest, called angina. Angioplasty or coronary artery bypass are the operations often used to cure this pathology. The first consists in enlarging the vessels using a balloon meanwhile the second consist in using a healthy vessel taken from the same patient from a different area of the body and used it to bypass the occlusion that causes IHD. However, these operations cannot be done in patients suffering from health problems or in cases where the risk is too high or they would not help in treating angina [38].

MLR consists in drilling the left ventricle by vaporizing the muscle and so make a 1-mm transmural channel by mainly using three different kinds of lasers like CO2, Holmium:YAG [39] or excimer [40] lasers, where the last two are realized in fiber technologies and could be useful for percutaneous approaches. After this channel is made, the oxygen-rich blood coming from left ventricle start to flow inside the muscle walls restoring the oxygen provision and instantaneously improving angina. The difference among lasers is in the wavelength and how the radiation interacts with the tissue. It was noticed [41] that the two most used lasers for this kind of operation (CO2 and Ho:YAG) have different effects when fired on the myocardium. CO2 lasers can create a channel by using a single pulse to traverse the myocardium, as opposed to Ho:YAG that needs multiple blast-like pulses resulting in different spot size and damage on the tissue. Although the CO2 lasers need only one pulse, the spot size is larger than the one of Ho:YAG but the latter creates more necrosis tissue, thus increasing the supply of collagen and making the zone more fibrous which impacts the contractile function of the heart without improving the angiogenesis. Indeed, comparison studies [42] demonstrated that the angiogenesis is greater in CO_2 lasers than in Ho:YAG.

Two different techniques are used to perform myocardial revascularization, and both involve different lasers and have a different degree of invasiveness.

Trans Myocardial Laser Revascularization (TMLR). In TMLR a CO_2 probe is placed directly on the myocardium [Figure 2-1] and controlled by a computer which synchronizes pulses with the

heartbeat. Each pulse is fired when the heart is in systole because the ventricle is filled with blood and the heart walls are the thickest thus preventing abnormal heart rhythms and damage to muscles. To check if the channel is made an intraoperative transesophageal echocardiography (TEE) is used. Ho:YAG laser [Figure 2-2 (a)] is used too and, as already said, it requires multiple pulses which do not require heartbeat synchronization and TEE confirmation. This is because Ho:YAG light is delivered through an optical fiber and it needs to puncture the epicardium and to advance forward through the walls once each pulse is fired. Normally, 25 to 50 channels are made on the entire left ventricle, and digital pressure is needed to obtain hemostasis which is reached shortly. This technique requires a thoracotomy through the fifth intercostal and the dissection of the pericardium making this procedure very invasive. Sometimes a less-invasive technique is used by exploiting thoracoscopic approach [43].

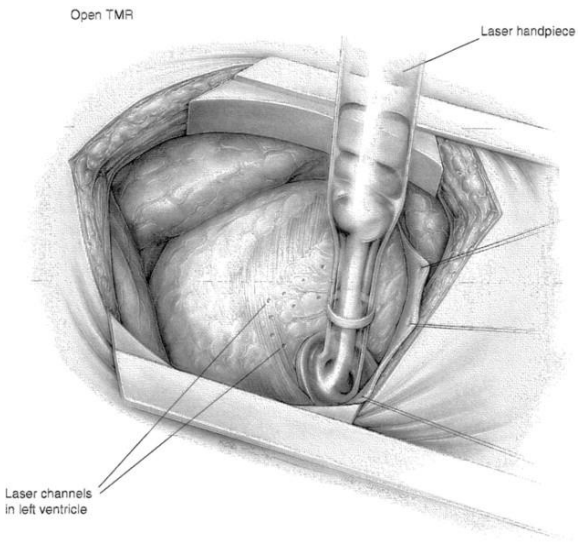

Figure 2-1 Trans Myocardial Laser Revascularization with CO2 laser [43]

Percutaneous Myocardial Laser Revascularization (PMLR). As opposed to TMRL, PMLR [Figure 2-2 (b)] is only performed by using a Ho:YAG laser and has no need for a thoracotomy and pericardium dissection because, being delivered by optical catheter-based fiber, the laser reaches the left ventricle by passing through the femoral artery. Up to 20 channels of about 5-6 mm depth out 8 mm walls thickness are then made by firing pulses to the endocardium.

Positioning of the fiber is followed by fluorescence technique but sometimes, to minimize its use, an electromechanical mapping system consisting of a real-time 3D imaging of left ventricle allows catheter tracking [44]

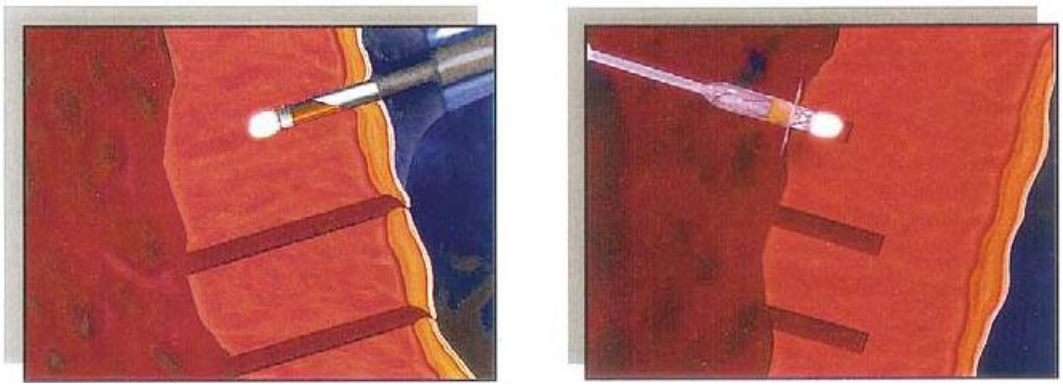

(a) (b)

Figure 2-2 Trans Myocardial (a) and Percutaneous Myocardial (b) laser revascularization with Ho:Yag laser [45]

Although it is known that MLR works for the treatment of inoperable IHD and angina, the mechanism on how this happens it is not well known but many hypotheses were made. Initially, it was thought that these channels remain patent thanks to the high pressure of the left ventricle that also helped to bring blood to the ischemic area, but this was disproved by a study [46] that found fibrous scars on the walls of the channels. However, the most accredited hypothesis supported by same study, is that this channel activates the auto-repair mechanism of wound that results in an increased angiogenesis. This mechanism together with the formation of fibrous scars suggests that laser necrosis myocytes start an inflammatory response that ends in angiogenesis and a better myocardial microperfusion.

Possible explanations for the reduction of angina could be found in the denervation of the myocardium due to the laser. Indeed, studies [47] demonstrated a significant improvement in symptoms after MLR and, performing it with a Ho:YAG laser on a canine heart, they found by microscopic analysis that it can damage or destroy nerve fibers.

ii. Laser-assisted vascular welding (LAVW)

Anastomosis is the operation of connecting two parts of vessels and it is a common operation in cardiovascular surgery. Conventional suture anastomosis consists in sewing together both ends of a truncated vessel or both sides of a longitudinal cut. This technique can, however, bring some disadvantages like foreign body rejection, liquid leakage, and slow healing but, to overcame these problems as well as to perform a less invasive operation, LAVW was introduced and refined through time [48]. This way of vessels bonding is based on sutureless coaptation by photothermal or photochemical processes in which radiant energy in converted into heat by mean of endogenous chromophores like water or pigments or exogenous chromophores applied in the solder, that enhances the denaturation of proteins and helps to bond tissue. The goodness of bonding is then measured with the leaking point pressure (LPP) calculated by a technique consisting in a colored saline solution continuously perfused while tracking the pressure (in mmHg) and until there is a pressure drop that corresponds to a leakage from the anastomosis. It will result in a rising and falling pattern of the pressure in which the maximum point is then considered as LPP and give an idea of the strength of the welded point.

The traditional LAVW however (i.e. the one without any additional solder), have some drawbacks like a low welding strength that needs additional suture to reinforce the anastomosis that then makes this technique pointless. Furthermore, an extended heating damage can cause intimal hyperplasia, thrombosis or aneurysm formation [49]. This technique was then improved to increase the welding strength and to limit heating damage by using a solder-enhanced LAVW (sLAVW) or a scaffold- and solder-enhanced LAVW (ssLAVW).

LAVW. Standard LAVW is based on photothermal effect enhanced by the absorption of photons by water, which in this case acts as an endogenous chromophore. The conversion of photon energy into heat makes the local temperature increase locally by subsequently altering the

vessel proteins. This alteration leads to a collagen cross-link between the two sides of the wound that need to be closed.

The amount and the link strength of the collagen, depend on how high temperature is and how it is distributed, features that are in turn dependent on laser source and the tissue interaction. The deposition of radiant energy is influenced by the absorption coefficient induced by water (or another chromophore) that also determines the Optical Penetration Depth (OPD) of a laser at a certain wavelength. The scattering index (SI) instead, is controlled by the macromolecular structure of the tissue and determines how radiant energy is diffused inside. After that, also the lasing parameter influence the heat distribution that is proportional to the laser irradiance (power (W)/spot area (cm^2)), exposure (irradiance x time (s)) and lasing mode (continuous or pulsed). The resulting temperature should be kept around 65° and 75° to have a good collagen link and low thermal damage. As already mentioned, despite the efforts to control the thermodynamic of the laser-tissue interaction, the thermal damage is high and the collagen cross-link is weak, so much that a stay suture is needed nullifying the use of LAVW.

sLAVW. To overcome the need of additional stay suture, laser tissue welding should be made stronger by enhancing the heat distribution and reducing the heating damage. For this purpose, a thin layer of protein solder (either liquid, solid or semi-solid) is used at the interface of the vessels to join, then the denaturation of proteins induced by laser irradiation will result in a cross link between proteins in the tissue and the solder. The fortifying effect is then due to the adhesive bonding between proteins in solder and vessel surface and the cohesive bonding between the solder proteins. The photocoagulation of the solder could be controlled by adding an exogenous chromophore such as Indocyanine green (ICG) or methylene blue, that allow the absorption of light in the visible range thus causing radiation absorption only in the thin layer of the solder and so shielding the vessel from thermal damage.

The target of this technique is to favor the heat generation between the solder-tissue interface so that the radiation would be uniform through the entire film thickness. To do that, the

concentration of the chromophore should be varied in order to obtain this uniform absorption. A low chromophore concentration leads to a low light absorption and a consequent low heat generation, so the denaturation of the proteins is insufficient, and the quality of the weld is poor. Also, a high concentration is to be avoided because, in this case, absorption is performed mostly in the superficial layer of the solder bringing optical shielding of the solder-tissue interface with a subsequent insufficient cross-link.

The heat distribution throughout the solder is also an important factor for a good welding and is influenced by its thermal properties. It has been demonstrated [50] that solder containing a concentration of albumin greater or equal than 50% has a better heat distribution that allows coagulation of entire solder and transmission of heat at the interface, granting higher cross-linking of albumin and tissue collagen. The best albumin solder for this kind of operation is derived by the Bovine Serum Albumin (BSA) that has the lowest thermal capacity among other kinds and requires the least energy to coagulate, thus preventing the risk of thermal damage.

Although the use of a solder improves the vessel welding by accurately controlling the heat distribution, it presents some practical drawbacks. Indeed, liquid solders leakage leads to inconsistent results, and the rigidity of solid ones interferes with cardiovascular applications.

ssLAVW. ssLAVW was introduced to overcome the leaking problem of the liquid solder in sLAVW. A scaffold made by a biocompatible semi-porous polymer is plunged in a solder, placed on the area to close and irradiated. In this way, besides the liquid retention, the scaffold provides a fortifying effect to the whole solder.

Anyway, the use of the scaffold modifies the optical property of the solder by increasing the SI in proportion to the thickness and the polymer fiber density. This change in the structure requires then a higher exposure than sLAVW to obtain an optimal soldering strength.

b. Photonics for Intravascular imaging and sensing

Besides the surgical branch, light-based technologies are also employed for detailed imaging and sensing of the cardiovascular system. Thanks to the small dimension of fibers, it is possible to realize catheter-based probes that can provide and inside precise view of the cardiovascular apparatus for an accurate diagnosis. In the following pages, three main technologies will be described, which use three different principles to gather useful information on the condition and composition of vessels.

i. Intravascular Optical Coherence Tomography (IVOCT)

Until not so many years ago, intravascular imaging was based on ultrasound techniques that provided cross-sectional images of vessels. These techniques helped to improve percutaneous coronary intervention (PCI) and the understanding of coronary diseases. But, in 1991, Huang et al. [51] first reported the birth of this new light-based imaging technique called Optical Coherence Tomography, that was gradually preferred to intravascular ultrasound (IVUS) for some applications. The OCT could now provide a resolution 10 times higher (up to 10 µm against 100 µm) and an imaging acquisition 40 times faster than IVUS.

Basic Principles. The OCT is basically based on interferometry. Light from a NIR source, typically ranging from 1250 to 1350 nm, is splitted and then sent to the vessel wall (sample arm) and to a reference mirror at a predetermined distance (reference arm). The light backscattered from the vessels wall, and the light reflected from the reference mirror are then collected and recombined by a detector resulting in a pattern of high and low intensity, which is the interference pattern. This pattern is then analyzed to obtain the amount of backscattered light in function of delay time or depth within the tissue (A-line). Cross-sectional images are obtained by rotating the optics and recording A-lines as the beam is scanned around the walls.

Earlier IVOCT analysis was performed in time-domain (TD-IVOCT), which means that the interference signal is derived by one NIR wavelength at a time. This technique was slow if

compared with IVUS and then required an occlusion with a balloon [52] to clean vessel from the blood as light could be scattered, an operation that was not always possible and that could increase the risks of ventricular defibrillation. The introduction of the Frequency Domain IVOCT (FD-IVOCT) was so a key milestone for the clinical adoption of IOVCT as it provides A-lines at a faster rate than TD leading to faster 3D pullback imaging without needing vessel occlusion but just using a transparent media such as Lactated Ringer's or radiocontrast. As opposite to the TD analysis, FD analysis measures the interference signal of the whole spectrum of the NIR source by using Fourier transformation at a single time [53].

Spatial resolution in OCT has two directions: axial, that is parallel to the light beam, and lateral that is perpendicular. Axial resolution is limited by the spectral bandwidth and is typically around 10 μm. Lateral resolution is instead limited by the spot size that depends on the distance from the focus and its depth. The best resolution is so obtained at the focal point of the lens (typically 1 to 3 mm from the catheter cover) in which the spot diameter d_0 is minimum and decreases as the spot size increases moving towards the vessels` walls. Moreover, lateral resolution is influenced by the number of A-lines acquired for each rotational scan, because with an insufficient number it could not be possible to resolve small objects.

The composition of the tissue under measurement can also affect the imaging process because of the variation of the refractive index (RI) that changes accordingly to the material. As it is known, the speed change of the light transmitted and backscattered, influences the delay time and so the actual distance of the tissue. A correction of the RI should then be provided in order to have a correct path, eventually with techniques able to estimate the real value, because the higher is the precision of the RI the more accurate is the measurement. The backscattered light collected by the catheter is also dependent on the difference between the change of RI at the interface of two different tissues (optical impedance) and the position in respect to the direction of light. The intensity of the OCT image is proportional to the RI difference and is

higher if a planar structure of the tissues, large compared to the wavelength, is perpendicular to the beam direction.

Also, the penetration depth, that is how deep the OCT can see inside the vessel wall, is influenced by the composition. Indeed, the light that passes inside the wall undergoes scattering and absorption effects that attenuate the light. For example, tissues like lipids have a stronger attenuation than collagen or calcium. This inhomogeneous distribution of tissues may vary the penetration depth of IVOCT that ranges from 0.1 to 2 mm. Moreover, blood strongly attenuates light before reaching the walls, which is why this technique needs a transparent liquid to flush away the blood while measuring.

Image analysis. The typical image of a normal vessel shows areas with different light characteristics which refer to different layers of the vessel. In an image of a healthy vessel, these layers can be distinguished according to their attenuation and reflectivity. E.g., in [Figure 2-3] an Internal Elastic Lamina (IEL) is characterized by a high reflectivity as well as the External Elastic Lamina (EEL), opposite to the media (M) that has a low reflectivity.

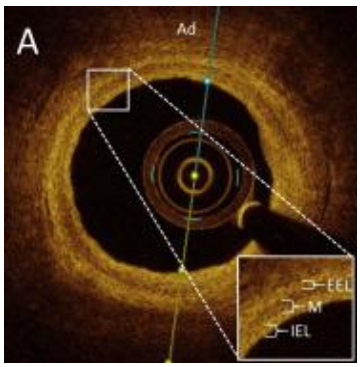

Figure 2-3 Cross-sectional OCT image of healthy segment of coronary vessel presenting the internal elastic lamina (IEL), the media (M), external elastic lamina (EEL) and adventitia (AD) [54]

Same method, together with a strong experience of the operator, is used to distinguish another type of tissues that can be found in an atherosclerotic vessel, as OTC offers the possibility to recognize lipid-rich, calcified and fibrotic lesions. Analysis of the plaque is indeed based on homogeneity, reflectivity, and demarcation from other structures. Lipid deposition is, for

example, characterized by diffuse edge, high reflectivity, and high attenuation as opposite to calcium that present sharp edges, low reflectivity, and low attenuation. Fibrotic tissues are instead visualized as a homogeneous zone with low attenuation and high reflectivity [Figure 2-4].

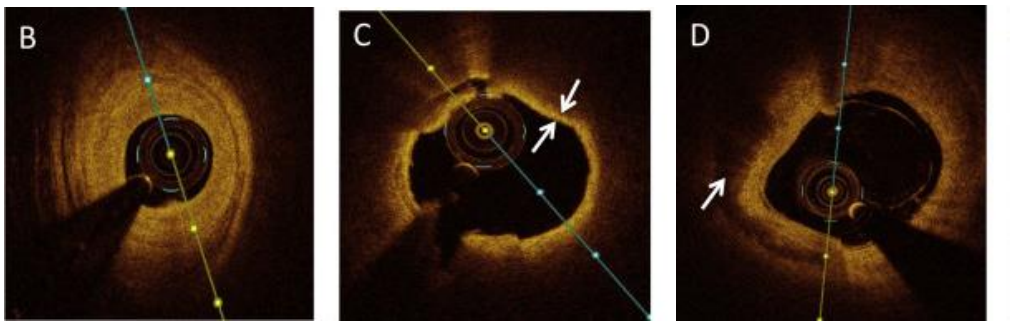

Figure 2-4 (B) Cross-sectional OCT image of fibrotic lesions. (C) Cross-sectional OCT image of lipid-rich lesion covered with thin fibrous cap atheroma (TCFA – white arrows). The image also presents small red thrombi. (D) Cross-sectional OCT image of calcification (white arrow) [54]

At last, IOVCT imaging it can detect vulnerable plaques prone to rupture. A vulnerable plaque is composed of a thin fibrous cap <65 µm, a lipid core, increased vasa vasorum and macrophage infiltration. The rupture of the thin fibrous layer is responsible for several problems like sudden cardiac death, acute coronary syndrome, and acute myocardial infarction. So, OCT became an important instrument that, thanks to its high resolution, can measure the thickness of the fibrotic layer.

ii. Catheter-based Near Infrared Spectroscopy (NIRS)

In the quest for a viable way to find vulnerable plaques, made its appearance also the Near Infrared Spectroscopy (NIRS). The idea lies on the base that NIR should provide information about the chemical composition of plaque by providing a "chemogram" of the wall of the artery that should be used as an index of vulnerability.

NIRS principles. The principle on which NIRS works on is the characteristics properties of *absorbance* and *scattering* of NIR light (from 800 nm to 25000 nm) owned by different substances. The absorbance is due to some molecular bonds, such as CH, OH, NH and others, which vibrational frequency is the same of the light hitting them. By illuminate a certain substance with broadband light and collecting light that returns back, we obtain an absorbance spectrum that indicates how much light has been absorbed for every wavelength of the broadband signal, thus providing information on which particular chemical composition the substance is formed [Figure 2-5].

Scattering is instead a deflection on which light undergoes when hitting cellular or extracellular structures. Because it varies as a function of wavelength and tissues, it is also a useful source of information about the chemical composition. However, scattering is also the cause of most of the loss of emitted light, so it requires an increase in the power of the source or the sensitivity of the detector.

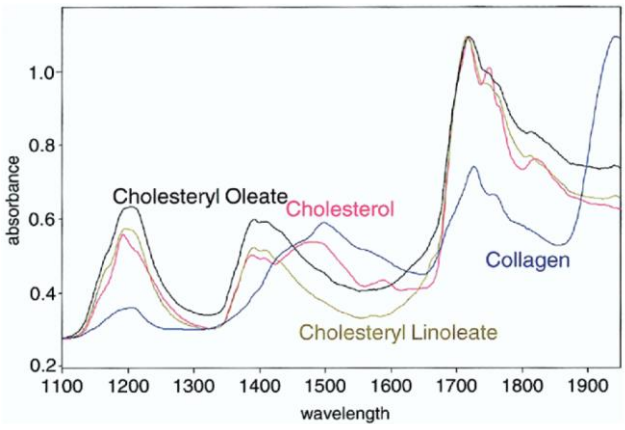

Figure 2-5 Near-infrared spectra of various pure substances possibly related [55]

Once a spectrum of an unknown tissue is provided, multivariate calibrations techniques known as “chemometrics” [56] are used to identify the chemical components. In the case of catheter-based NIRS for Lipid core–containing coronary plaques (LCPs) search, the probe performs a circular scan during the pullback, thus providing a complete analysis of the vessel walls and a chemogram as in [Figure 2-6]. This two-dimensional image shows where there is a high probability of finding an LCP according to the pullback distance *(x-axis)* and the rotational degree *(y-axis)*.

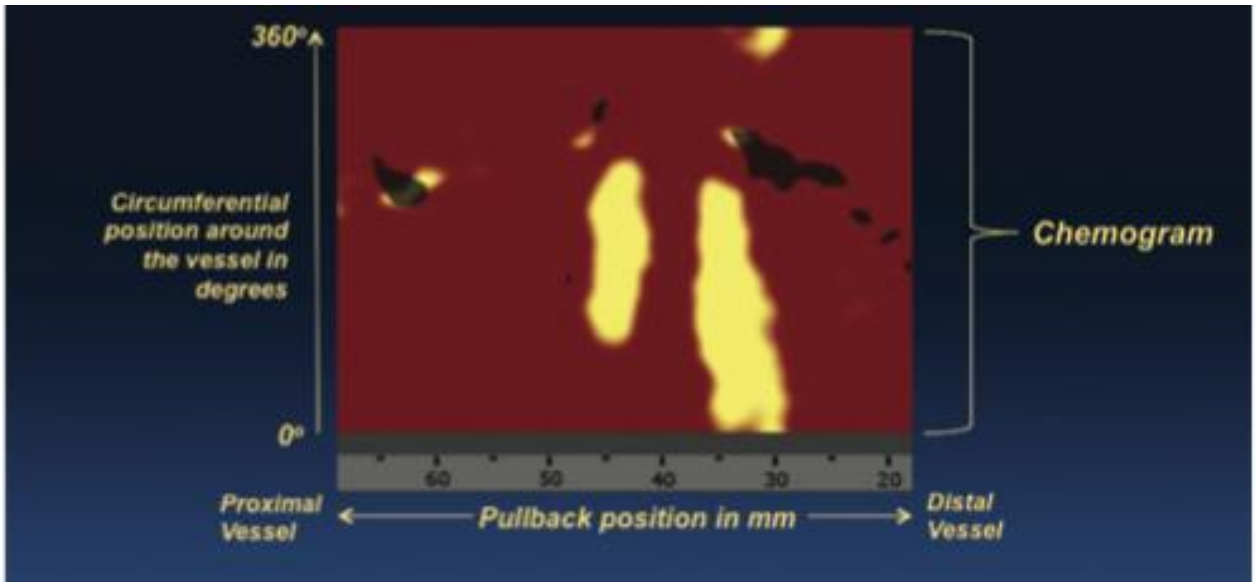

Figure 2-6 two-dimensional map of the artery that indicates the location of lipid core plaque [57]

With the ratio between the area containing the LCP and the total area, NIRS can also provide the calculation of lipid core burden index (LCBI), a measure of how much the LCP is extended in the region of interest, as opposed to IVOCT that is limited by its low penetration depth. Furthermore, NIRS does not need vessel occlusion or blood removal thus reducing the complexity of the operation.

To take advantage of both IVOCT and NIRS, a system which combines both techniques was proposed [58]. Thanks to this integration, the resulting analysis can provide information on both

dimension of tissues that compose the plaque, and their chemical composition. An example of the result is shown in [Figure 2-7] in which we can see both the vessel image from OTC and a superposed chemogram from NIRS. In this image, the presence of an LCP can be seen watching the area indicated by the arrow and the absorption spectrum around the scan.

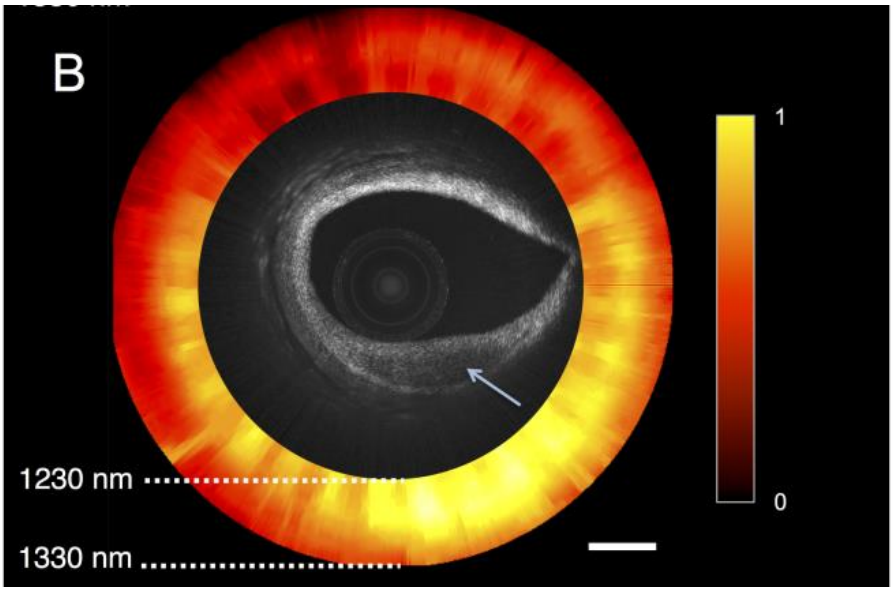

Figure 2-7 OCT-NIRS images of cadaver coronary artery ex vivo. OCT images show lesions with reduced backscattering. NIRS image shows absorption spectra of tissue versus wavelength, representing the total attenuation normalized for the entire data set;

iii. Optical fiber pressure sensor (OFPS)

Blood pressure measurement is a very important parameter in the medical field, as it provides information on the pathophysiological status of an organ. Indeed, depending on the area and on the pathology, blood pressure undergoes different variations that need different precision of measurement as suggested by Clause and Glott [59] that recommends to divide blood pressure into three domains: *low pressure domain* (capillaries, brain, urinary bladder, and muscular compartments); *medium pressure domain* (circulatory system including the heart), and *high pressure domain* (load bearing structures like hips and knees).

Most of the previously realized pressure sensors rely on the conversion from physical to electrical signal by mean of piezoresistive, piezoelectric or capacitive principles. These sensors

were limited by a large dimension that can restrict blood flow and can anyway be damaged or destroyed in case they are used in combination with Magnetic Resonance Imaging (MRI) or radio-frequency ablation techniques.

Optical Fiber Pressure Sensors (OFPS) are so an alternative to the classical electrical sensor and, as the name suggests, are based on a single or multiple fiber systems so they present very small dimensions and are immune to electrical interference. Early stage OFPS were based on intensity change, by both modulation and attenuation principles, and represented a low cost and simple design alternative. Later, the advent of Fiber Bragg Grating (FBG) sensors pushed to use this technology also in the pressure sensing as it provided an intensity-independent output. At last, improvements on microfabrication technologies made possible the fabrication of Fabry-Perot cavities and then the realization of Extrinsic Fabry-Perot Interferometer (EFPI) sensors that provide an intensity-independent output too and sensitivity and accuracy three order greater than FBG.

Intensity Based Pressure Sensor. The principle on which an intensity-based OFPS works is quite simple. The light coming from an external source is sent in a multimodal fiber to a reflecting diaphragm that deflects with pressure, then the light reflected from this diaphragm is collected by another fiber and sent to a photocell. The intensity thus depends on the distance between fibers, the core diameter, their numerical aperture and the distance from the diaphragm. As can be seen in [

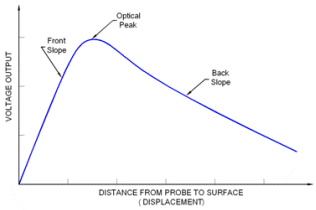

(A) *(B)* *(C)*

Figure 2-8], when the target is close to the fibers (A), coupled light is low or even zero if it is in contact with them. As the target moves away from the fibers (B), coupled light increases until

the diaphragm plane reaches the position in which the solid angles of the numerical aperture overlaps the most, then it starts to decrease again (C).

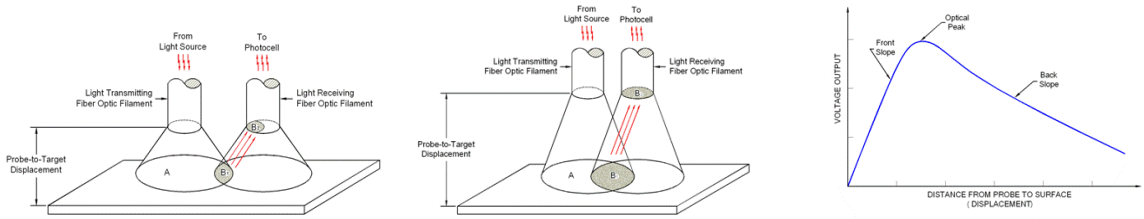

(A) *(B)* *(C)*

Figure 2-8 Examples of numerical aperture overlapping. (A) Target near to the fibers; (B) Target far from the fibers; (C) Diagram of the intensity vs the displacement of the target [60].

After designing the system for a selected range, pressure can be derived by considering only one monotone region of the curve and after calibration.

This technology is the cheapest among all the OFPSs, as it does not require expensive optical devices but only a LED and a photodiode to send and receive light through in a multimodal fiber. This simplicity anyway, is paid in terms of reliability as the components of the sensors are sensible to the external environment. For instance, light source and photodiode are sensible to aging and temperature, and so light from the source or the current from the photodiode can fluctuate. Again, the diaphragm can change its reflectivity because of thermal effects or oxidation and, depending on the material of which is made, thermal expansion could induce apparent pressure shifts. Furthermore, another source of light attenuation is due to fiber bending especially when large core ones are used to maximize light from the source. One possible solution could be placing the fibers in a rigid support, but this is not acceptable in cardiovascular applications where catheter need to be flexible to move through vessels. To help estimate bending losses, one or two non-sensing fibers can be added [61], although there is still some local micro-bending that can affect the measure. Anyway, this system provides an

adequate compensation for Intracranial Pressure (ICP) monitoring, that is the major application in which OFPS are used.

Fiber Bragg grating pressure sensing. A Fiber Bragg grating (FBG) is formed by a periodic change of the core refractive index n_{co} with a period Λ (pitch). Light traveling through the grating is reflected at each grating period resulting in a narrow-band reflection at the Bragg wavelength λ_B thus defined:

$$\lambda_B = 2\, n_{eff} \cdot \Lambda$$

where n_{eff} is the effective refractive index of the core in the grating region. Using some techniques to convert pressure into strain in the direction of the fiber axis, will result in a variation of the length in that region and so on the grating pitch [Figure 2-9]. Pressure is then calculated indirectly from the strain of the fiber that led to a Bragg wavelength shift.

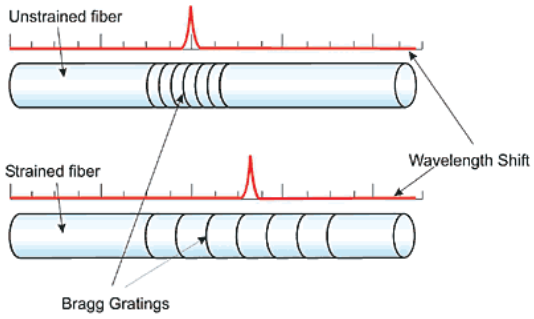

Figure 2-9 Fiber strain and wavelength shift

Among various approaches to convert pressure into strain, the most used consists in attaching the fiber to a membrane either orthogonally or in the membrane plane, or using some

assemblies that increase pressure sensitivity by some mechanical amplification scheme. The first approach implies bulky sensors that, although could work for high-pressure applications or where size does not matter, are not suitable for cardiovascular applications. The second approach instead allows slimmer designs by varying coating and assemblies but at the expense of the sensitivity.

Moreover, the huge problem with FBGs is that they are sensitive to temperature change in the same way as for strain, making very difficult separation of both contributes.

Finally, FBG present higher costs and limited applications compared to other OFPS techniques, which is why this technique has reached no high-volume commercial applications.

Fabry-Pérot pressure sensors. One of the best technologies for pressure sensing that gained high commercial success is certainly the one based on Extrinsic Fabry-Pérot Interferometer (EFPI). This success relies on providing a good design flexibility, besides offering multiple parameter measurements [62]. Substantially, an EFPI pressure sensor is composed by a vacuum cavity with a semi-reflective mirror end, thus forming a FP cavity, and a reflective membrane placed above it. A certain percentage of light traveling in the cavity passes through the semi-reflective mirror until it reaches the membrane [Figure 2-10]. In this way, the light travels for an additional path length of 2L, (where L is the displacement of the membrane) from the mirror end due to the external pressure, and so experiencing a phase difference.

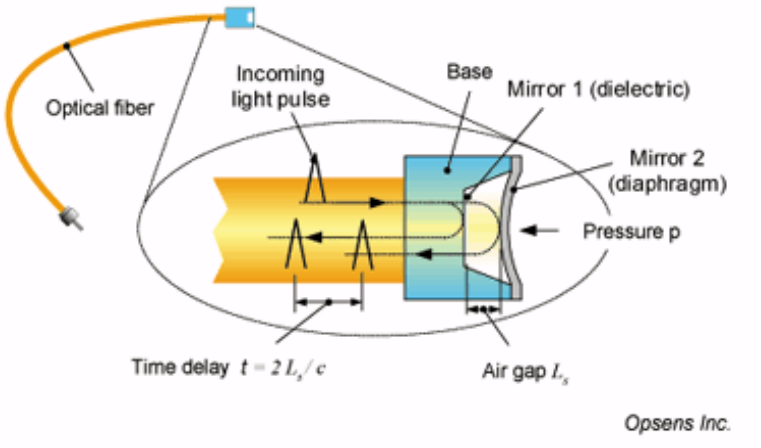

Figure 2-10 - Schematic of pressure transducer based on Fabry-Perot [63]

Usually, the source used in these systems is a white light or broadband one that results in an interference spectrum from which the displacement of the membrane could be detected by further analysis techniques. It is worth mentioning a patent from *FISO Technologies* that uses an interference pattern created in the FP interrogator by a Fizeau wedge that creates a linear variation of thickness. The intensity peak position of the cross-correlation of this pattern with the one generated by the in the FP cavity will correspond to the length difference brought by the membrane displacement.

The design flexibility of the EFBI pressure sensor consists in using different materials and dimension accordingly to the application and the sensitivity required. For cardiovascular applications, a suitable EFBI pressure sensor with a diameter of 125 µm diameter has been reported [64] . Although it is not a problem for many commercial application such industry sensing, the size of the sensor is an important feature for medical applications, as probes should be integrated into a catheter for reliable *in situ* pressure detection.

c. Background knowledge

In this section, there will be a brief explanation of some concepts that the reader could be unfamiliar with. In particular, it will be shown the theory behind the triangulation and the PWV because this is crucial for a complete understanding.

i. Pulse Wave Velocity and Arterial Stiffness

Arterial stiffness is a physical parameter that quantifies the “rigidity” of the arterial walls, which are constituted of three layers: tunica intima, tunica media, and tunica adventitia. Abnormal arterial stiffening is generally caused by degenerative changes in the composition and/or architecture of the cells and extracellular matrix in the “tunica media” [65], which is the thickest of the three layers and that is also rich in smooth muscle cells, helping to control the caliber of the vessel.

In a healthy cardiovascular system, elastic arteries undergo a significant dilatation upon arrival of the pressure wave produced by the heartbeat, and produce a stiffness gradient from proximal to distal arteries, creating a wave reflection phenomenon. When arteries become rigid, the speed of propagation of the arterial pulse through the aorta increases, creating an increased speed of the forward traveling waves with an earlier reflection from the periphery. Reflected waves arrive at the heart in systole instead of diastole, creating an elevated aortic systole pressure and a left ventricle overload: the heart must provide an additional effort because of the increased impedance of the arterial system, and increase aortic systole pressure.

Arterial stiffness is influenced by aging, atherosclerotic risk factors and arterial inherited diseases, and is a recognized predictor of cardiovascular mortality [66]. Indices of aortic stiffness are being used for preclinical diagnosis of arterial disease and for the monitoring of the responses to treatments. In the clinical guidelines from the European Society of Hypertension and the European Society of Cardiology (ESC), the evaluation of arterial structure and function has been indicated when treating hypertensive patients [67]. A simple and robust method for evaluating aortic stiffness is the measure of the pulse wave velocity (PWV), which is the speed of the pulsatile wave traveling along the viscoelastic wall of blood-filled arteries [67]. As the arterial functions may show regional variations, depending on age, gender and underlying diseases, the possibility to evaluate local arterial stiffness at specific sites is of major interest [68]. The mathematical relation between AS and PWV is characterized by the Bramwell-Hill equation and is defined by the equation reported below, being β the arterial stiffness, P_s the systolic blood pressure and ρ the blood density (1050 kg m^{-3}).

$$PWV = \sqrt{\frac{\beta P_s}{2\rho}} \ (\mathrm{m/s})$$

The PWV is typically evaluated by measuring the time interval between the arrival of the pressure wave in the carotid and femoral arteries, thus providing the "average PWV" in the thoracoabdominal tract of the aorta [69].

Different contact-requiring methods can be used to measure PWV, and those based on pressure sensors are today considered the gold standard methods. The 3 main devices currently used in clinical and research settings are PulsePen [70], Complior [71], and SphygmoCor [72]. PulsePen is composed by a tonometer, an instrument that measures the pulse pressure by compressing it on the bones underlying and integrated an electrocardiogram (ECG) unit. Complior uses two dedicated piezoelectric pressure mechanotransducers directly applied to the skin in a simultaneous measurement of pressure pulses. SphygmoCor analyzes the pulse wave of the carotid and femoral arteries, estimating the delay with respect to the ECG wave and calculating the PWV. Another possibility is given by using ultrasounds to estimate the local PWV as the ratio between the change in flow and the change in cross-sectional area during a cardiac cycle, calculated by echo-tracking (Aloka ultrasound alpha 10) [69]. Even in this case, it is important to highlight that a physical contact between the sensor and the patient is needed and that the pressure applied on the patient tissues can obviously modify the PWV estimation.

Typical values of PWV reported on [73] are showed in

Table 2-1

Age category (years)	Mean (±2 SD)	Median (10–90 pc)
<30	6.2 (4.7–7.6)	6.1 (5.3–7.1)
30–39	6.5 (3.8–9.2)	6.4 (5.2–8.0)
40–49	7.2 (4.6–9.8)	6.9 (5.9–8.6)
50–59	8.3 (4.5–12.1)	8.1 (6.3–10.0)
60–69	10.3 (5.5–15.0)	9.7 (7.9–13.1)
≥70	10.9 (5.5–16.3)	10.6 (8.0–14.6)

Table 2-1 Distribution of pulse wave velocity (m/s) according to the age category in the normal values population (1455 subjects)

ii. Laser Triangulation

For our project, we choose to use laser triangulation because of its simple configuration and because, by using a CMOS sensor, it is easily reconfigurable and scalable if more sources are needed thus keeping costs low.

Because the device uses this technique to evaluate the response to the systolic pulse, I will elaborate now its basic principles. The principle behind the triangulation method is to form a triangle between two observers placed at a known distance ***b*** [Figure 2-11], thus forming the base of the triangle, and the object to be measured placed at the remaining vertex. By measuring the consecutive angles ***α*** and ***β*** between the object and both the observers, we can define the distance ***d*** by putting in a system two simple trigonometric relations like:

$$d = b_1 \cdot \tan\alpha$$

$$d = b_2 \cdot \tan\beta$$

where b_1 and b_2 are the distances between the observers and the intersection of ***b*** and ***d*** for which the sum is equal to ***b***.

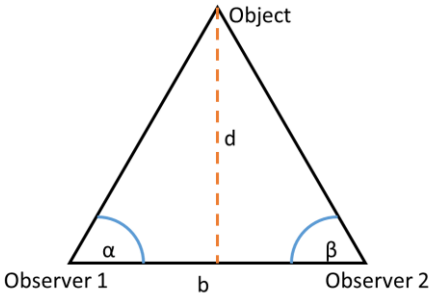

Figure 2-11 - Reference triangle

In a laser triangulation system, one of the observers is composed by a laser source and the other by a CCD/CMOS sensor as in [Figure 2-12]. The focal point of the lenses is taken as a zero-point reference and when the object under measurement is moving, the angle between this and the CCD/CMOS sensor changes, such as the point at which the laser hits the sensor. The spot (e.g.

the pixel) on which the laser hits the sensor varies according to the displacement of the object thus making possible to accurately know the displacement of the object.

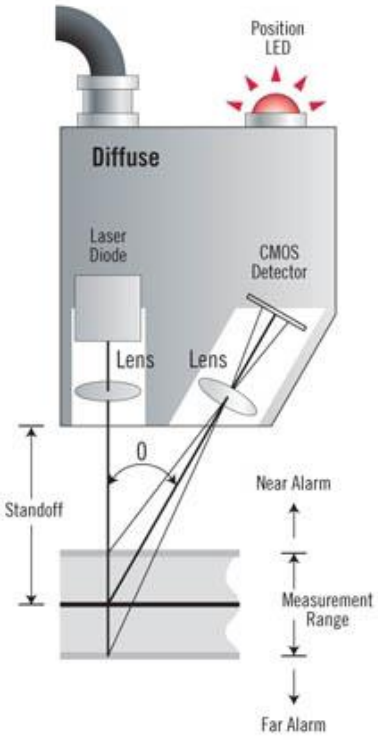

Figure 2-12 Laser triangulation system [74]

This technique allows by design a contact-less measurement without influencing the object movement, making it ideal for vibration measurement as no mass it is added to the system.

d. Advantages

i. Light technologies

As we could see from the above presentation of the most used light-based technologies for cardiovascular diagnosis and intervention, the major advantages of this kind of instruments rely on their versatility, robustness and precision compared to traditional technologies.

For example, fiber-based catheter used in surgery provide an extreme localization of the laser beam thus allowing to precisely incise or cauterize a tissue without affecting the surrounding

area and avoiding complications or damages as well as reducing trauma and decreasing hospitalization time.

Previously presented imaging techniques instead, provide higher precision than traditional method such X-ray or ultrasonic imaging, which respectively provide only a projection of a vessel or a lower precision of an order of magnitude. A higher resolution mean that more irregularity or pathologies affecting tissues can be characterized and threated in the same session thus averting future complication and hospitalizations.

To conclude, light-based technologies provide more accurate method of analysis and threating of the cardiovascular disease that translate to faster and shorter hospitalization. This mean that, reducing the time in which the patient need diagnosis and health cares for the most invalidant disease in the world, lot of resources can be saved thus lowering costs for health systems.

ii. Nistas project

As mentioned before, the final product of the Nistas project will be a light-based device called Vasculight that aim to a fast measure the Pulse Wave Velocity (PWV) of the blood pressure wave passing inside the carotid related to the Arterial Stiffness (AS). A technology that allow an easy, safe and fast detection of PWV translate in the possibility to be diffused in point-of-care and hospitals allowing a rapid screening and assessment of the patient health, without involving resources that are more expensive and time-consuming. This could also lead to a constant monitoring of the cardiovascular health in order to avert possible complication or for a fast assessment of the effects of a cure.

The measure of the AS at local level, is of major interest [75] because arterial functionality may show regional variations, depending on age and underlying diseases. Currently method like ultrasound wall tracking method is extremely time consuming (40 – 60 min) and strongly operator dependent. These limitations restrict the routine daily application of the measurements, limiting the direct arterial stiffness measurement to selected patients.

The measurement of the PWV instead, is a more widespread and accessible technique for the measurement of arterial stiffness as well as the best predictor of cardiovascular mortality [76]. Today's gold standard method to measure PWV are contact method based on a "regional" evaluation of the carotid-femoral trait by using piezoelectric pressure sensors. Since there is no yet an available contactless technology, Vasculight will be designed to fill this gap that could lead to local assessment of the PWV and to an improved accuracy in the measurement (2.5% of Vasculight vs. 15-20% of other system).

3. NISTAS Project

In the previous chapter were described the mains Biophotonics applications in cardiovascular medicine, and their impact on cardiovascular diseases diagnosis and intervention was reported. As it could be noticed, the use of the light make surgeries and analysis less invasive and more precise than other methods, although sometimes drawbacks and costs not always make Biophotonics devices a convenient choice. Anyway, currently light technologies are used when the cardiovascular disease is already known or at least when there are already some symptoms and more tests should be performed to find what the specific problem is.

Generally, when symptoms arise, it could be already too late to prevent a disease, and there is no other way than to start a therapy or undergo an intervention. A good habit could be to check periodically one's health status but currently used methods of screening of the cardiovascular system need long waiting lists and a long time to be performed so vanishing the idea of frequent check-ups.

This scenario suggests the need for fast methods to easily have feedback on what are the physiological conditions of the cardiovascular system thus making its monitoring a real possibility. This is precisely the target of the European project NISTAS, which aims at the development of an instrument (named Vasculight) allowing fast, contactless and non-invasive monitoring of the cardiovascular system status by employing light technologies.

The principle on which this device relies is the detection of Pulse Wave Velocity (PWV), a well-known parameter for the evaluation of the arterial stiffness. PWV indicate the speed of the sphygmic wave traveling in the aorta, carotid or other arteries and, in the case of NISTAS, is measured by mean of an optical system that provides a contactless detection thus avoiding any contact-related artifacts. Arterial stiffness (AS) is a recognized predictor of cardiovascular risk and mortality, and it is also a potential marker for monitoring the beneficial effects of medical treatments for arterial diseases.

This chapter is, therefore, dedicated to the presentation of the project in which I worked during my Ph.D. It will serve as an exhaustive description to understand its composition, working principles and the impact that could have in clinical applications.

a. Prototypes Architecture and workflow

This section will describe the architecture of two prototypes used during the study of the system. The first one was needed to define a measurement workflow and a detection algorithm and was based on a commercial device. The second and final prototype was instead build to satisfy the technical requirements of the project when the workflow and the algorithm were well established.

iii. Prototype 1

For the preliminary study of the device, a commercial profilometer based on triangulation was used. It is constituted by two Keyence LJV-7080 [77] [Figure 3-1] optical heads and a mainframe interfaced with a PC to store data for a consecutive elaboration. Each head is a complete triangulator equipped with a blue light (405 nm) source that projects a line on the object under test to acquire a complete profile instead of a single point and a CCD sensor. Blue light is chosen because is not diffused under the skin, as opposite to red and infrared light, thus allowing a better resolution. Furthermore, blue light provides a better signal contrast in the case of strong ambient light as it lies at the edge of visible emission of conventional lamps and sunlight.

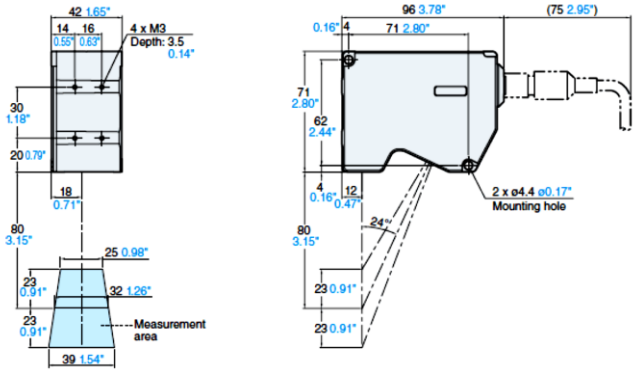

Figure 3-1 Keyence LJV-7080 head –technical data

The reference distance is placed at 80 mm from the output windows on the Z axis and the maximum span that could be detected is 46 mm centered on the reference distance, so -23 and +23 mm from it. The width of the laser line at the reference distance is 32 mm, and it varies from 25 mm to 39 mm in the measurement range. Moreover, this sensor allows a precision of 1 µm that is far beyond our requirements.

As mentioned above, the complete system [Figure 3-2] is composed of two optical heads (1) placed in a way that the distance between laser lines is 40 mm, supported by an articulated arm (2) that grants an optimal spatial positioning and a good stability against vibration during the measurement. The data acquisition unit (3), is demanded to manage both the heads, to acquire data coming from them at a sample rate of 1 kHz, and to send this data to the PC where it will be stored.

Figure 3-2 Complete system
1 – optical head with 2 laser sensors; 2 – support articulated arm; 3 – data acquisition unit; 4 – Elaboration and visualization system; 5 – cables.

iv. Prototype 2

The optical module (optical head) of the NISTAS prototype is depicted in [Figure 3-3]: LPS1 and LPS2 are the light-line projection systems and used to generate the two parallel beams which are to be directed onto the skin of the patient. D1 and D2 are the displacements to be measured along the two lines projected across the artery.

The camera lies on a plane perpendicular to the lines direction and is tilted by a 45° angle as shown in the right panel of [Figure 3-3]. The optical lenses mounted on the camera have been chosen in order to allow the imaging of both light-lines within the field of view and the depth of focus of the camera. The detection of the skin displacement is based on the light-line profilometry technique.

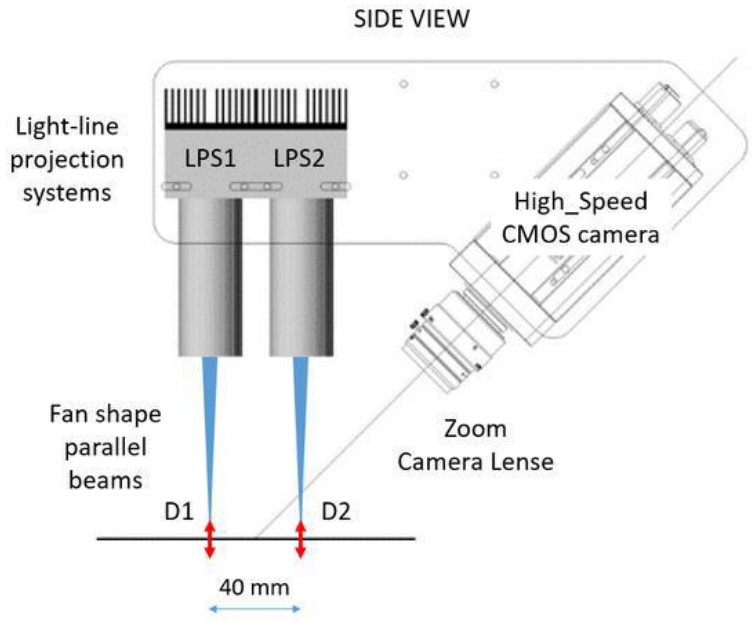

Figure 3-3 Mechanical scheme of the optical module.

The dual-line light projection system is based on LED sources, emitting at 460 nm (blue light), and generates two parallel fan-shaped beams through a custom-designed optics. At the working distance, the light lines are 25 mm wide (in the direction perpendicular to the figure plane) and 400 µm thick (along the horizontal axis in the figure).

The use of LEDs instead of laser sources allows avoiding the speckle pattern effect, typical of highly coherent radiations, that is caused by beam self-interference. The presence of speckle-pattern makes the intensity distribution severely non-uniform along the light lines, affecting the resolution of the triangulation system.

The monochrome high-speed camera included in the system (Ranger E40, produced by SICK A.G.) is specifically designed for laser line profilometry and is configured for “MULTISCAN” operation, allowing the simultaneous detection of the two light lines (i.e. of the two profiles). This special feature of the camera, allows to exploit the sensor in a very smart way: the 512x512 pixel COMS sensor is “split” into two separated areas (upper and lower), each one of dimension 512 x 256 pixels, allowing to detect the images of both lines and, then, to calculate the relative

profiles at the same time. With the chosen camera lens, the camera field of view (FOV) is about 50 mm × 50 mm at a focusing distance of about 100 mm.

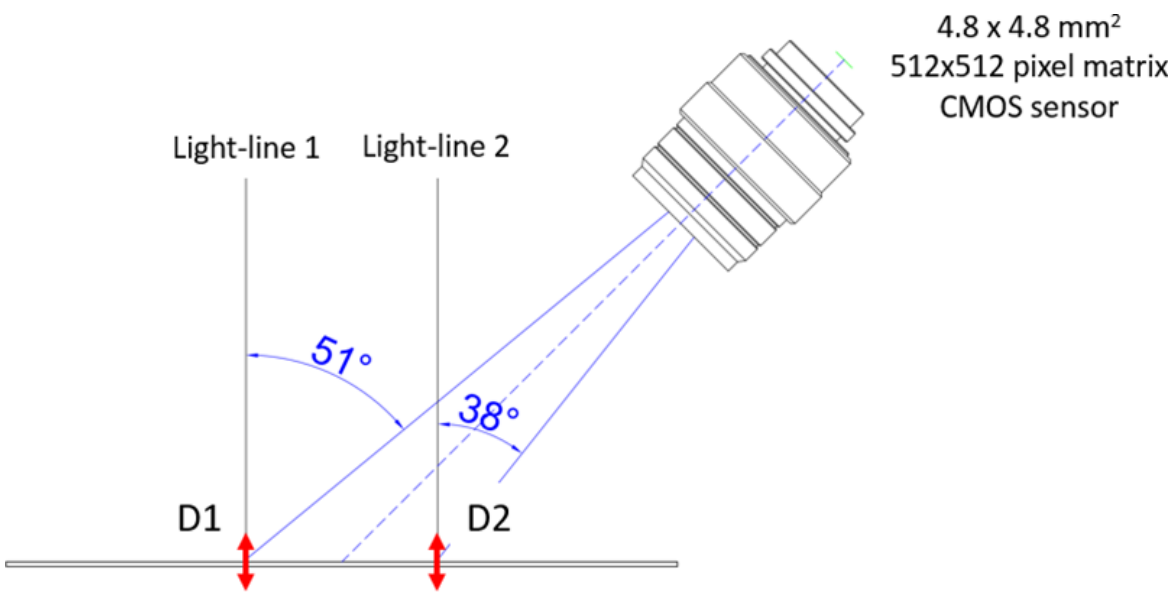

Figure 3-4 Directions of the projected light lines and of observations from the camera.

When the optical head is placed at the correct distance from the patient, i.e., with the external tubes of the LPSs at 80 mm far from the skin, the central axis of the camera passes through the middle of the two projected light lines. As explained in [Figure 3-4], the two light lines are seen by the camera sensor with and an angle of 51 and 38 degrees respectively, with respect to the vertical axis. In this condition, the projections of the displacements D1 and D2 onto the sensor can be calculated as:

$$D_{1\,sens} = \frac{D_1}{\sin(51)} \cdot \frac{SensorSize}{FOV}$$

$$D_{2\,sens} = \frac{D_2}{\sin(38)} \cdot \frac{SensorSize}{FOV}$$

Using equations 1 and 2, with *FOV* = 50 mm, *SensorSize* = 4.8 mm and using, as an example, D1 and D2 = 100 µm (i.e., the typical order of magnitude of the displacement induced by the pulse-wave travelling along the carotid path), the values of D1 and D2 projected onto the camera sensor are:

$$D_{1\,sens} = 12.3\ \mu m$$

$$D_{2\,sens} = 15.6\ \mu m$$

Considering that the pixel size of the CMOS sensor is 9.5 × 9.5 µm and that the camera is configured for using an embedded algorithm capable of improving the resolution of the displacement detection to 1/16th pixel, the displacement measurement of D1 and D2 can be achieved with an accuracy of about 10 microns. The average accuracy of the displacement measurement achievable with the triangulation system designed for NISTAS, considering an average inclination angle of 45 degrees, is thus 8.7 µm, as calculated from the following equation:

$$Accuracy = \frac{PixelSize}{16} \cdot \frac{FOV}{SensorSize} \cdot \frac{1}{\sin(45)}$$

iii. Procedure

The idea behind the calculation of the PWV is to use two laser or LED source at a known distance and then to detect the time needed by the traveling wave to pass from a line to the other. At this point, we will simply calculate PWV by dividing the distance length (L) between sources and the time (t_d) employed to cover that distance:

$$PWV = \frac{L}{t_d}$$

The measurement procedure is then based on performing this detection as comfortably as possible to avoid errors or inconvenience for the patient.

So, before performing a clinical survey, we defined a procedure that allows the system to provide reliable data with less noise as possible. This procedure is the same for both the prototypes because they share the same working principle and weakness.

First, the best position for the patient is to lay on the bed so to avoid any spurious movement that could be detected by the instrument. After the patient is in a comfortable position, his head should be slightly reclined to the back and to the opposite side of the measure (e.g. if the measure is performed on the right side of the neck, the head should be reclined to the left) thus making the positioning of the optical heads easier. Particular attention should be paid to not extend too much the carotid muscles because the elasticity of this latter could change and so the response of the skin to the pulse.

Once aforementioned requirements are reached, the device could be placed in order to perform the measure by taking care that the laser profile is positioned perpendicularly to the carotid, though no extreme precision in needed. Care should also be taken to isolate the device mechanically, as any contact with the patient or the operator should be avoided because it can induce spurious vibration.

A single measure lasts exactly 20s, so the sampling frequency should be regulated according to the system used. For the first prototype we used a frequency of 1 kHz and, in the case of the second prototype instead, we used a sampling frequency of 409.6 Hz because the image acquired is limited to the camera buffer size but this granted anyway a time resolution of 2.4 ms which is good enough.

To have an idea of the goodness of a measure, three detections for each side are performed. In this way, we can evaluate the reliability of the PWV value detected by comparing the three measured values and calculate their variance.

b. Algorithm

After the acquisition, data must be processed to calculate the delay of the traveling waves that pass under both lasers. Dealing with noise, spurious peaks and a traveling wave not perfectly perpendicular to both laser line, make this not an easy process. That is why the acquired profiles should be numerically managed to find a significant value.

Data from the device is presented as a matrix in which rows are the time sample, columns are the width samples and the value in each cell is the local height at that position and time.

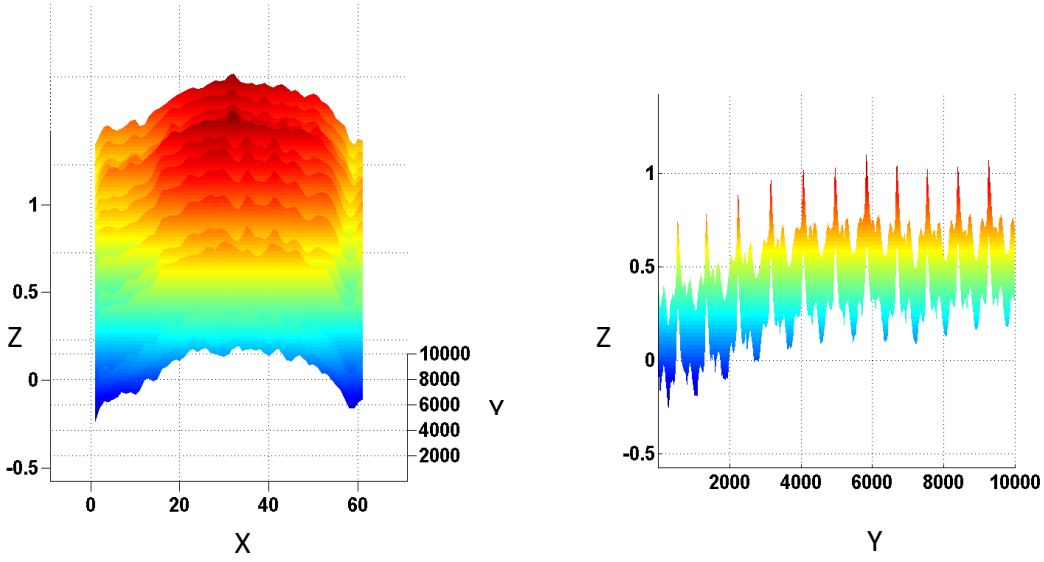

Figure 3-5 Graphical representation of an acquisition matrix. (Z) is the height in A.U., (x) the number of samples of the width and (Y) the number of time samples

A graphical representation of this matrix is reported in [Figure 3-7], in which it could be noticed the peaks corresponding to the pulses. Always referring to the graph, a curvature on both the profile in the z-x and z-y planes could also be noticed. These curvatures are related to the neck shape, for the z-x plane, and to the breath of the patient. The first step to being performed is to give to the graph a flat shape to make easy future elaboration. To do this, an average pattern is calculated by using a smooth function, and this is then subtracted from the original matrix thus having at the end a flat graph [Figure 3-8].

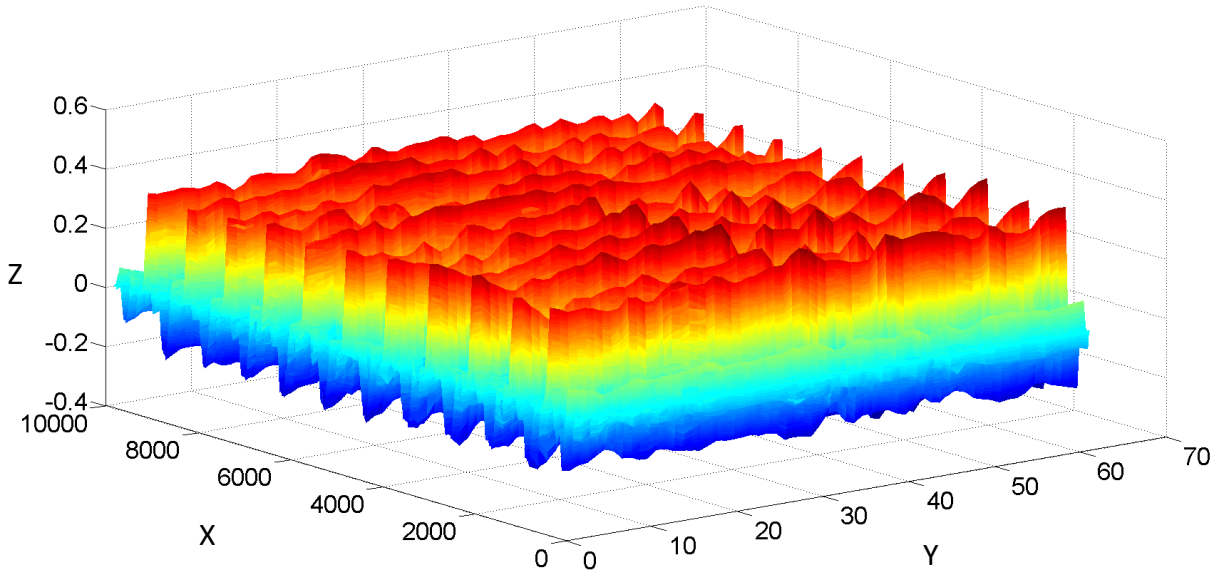

Figure 3-6 Graphical representation of the smoothing process. (Z) is the height in A.U., (x) the number of samples of the width and (Y) the number of time samples

Once we have this flat 3D signal, we can start to manage it to obtain the PWV value. Thanks to the acquisition of a complete profile, an area of the width in which the height is maximal for each of the two signals should be found. The problem now is that the carotid could be oblique to both the traces, so this maximal area could not be the same for both. Also, if the search of this area is made by considering only the height, the algorithm could run into error if there is a spurious maximum.

Therefore, what is done, is to split both matrices in 10 “spatial strip” each, that are a portion of the width that keeps the time evolution and then, for each strip, an average displacement-vs-time curve is calculated so to obtain a single waveform. There are some considerations to make with regards these waveforms. Once them are obtained, could be noticed that not every signal is perfectly smoothed and with the systolic peak well defined but instead an important amount is affected by some noise due to unwanted vibration, hairs on the neck or by the interferences with ambiance light. Furthermore, the composition of the neck could contribute to the goodness of the signal, because the elasticity of the skin, fat under the skin and tension of the muscles can influence the response to the pressure wave and so the peak revealed by the device

could be less sharp than we expect. Anyway, in the algorithm I implemented some functions that fit the pulse and so the information otherwise lost could be recovered. At this point, the algorithm chose among the strips the "best couple" in terms of spectral similarity, by calculating the spectral coherence [78] of each of the 100 possible couples (10 x 10) and taking the one with the highest degree of spectral coherence within the band of 20 Hz.

Spectral coherence is a measure of how much two signals are similar in frequency terms and is calculate by the following formula:

$$C_{12}(f) = \frac{\left|G_{1,2}(f)\right|^2}{G_{11}(f)G_{22}(f)}$$

The result of this calculation will produce the graphic in [Figure 3-7]

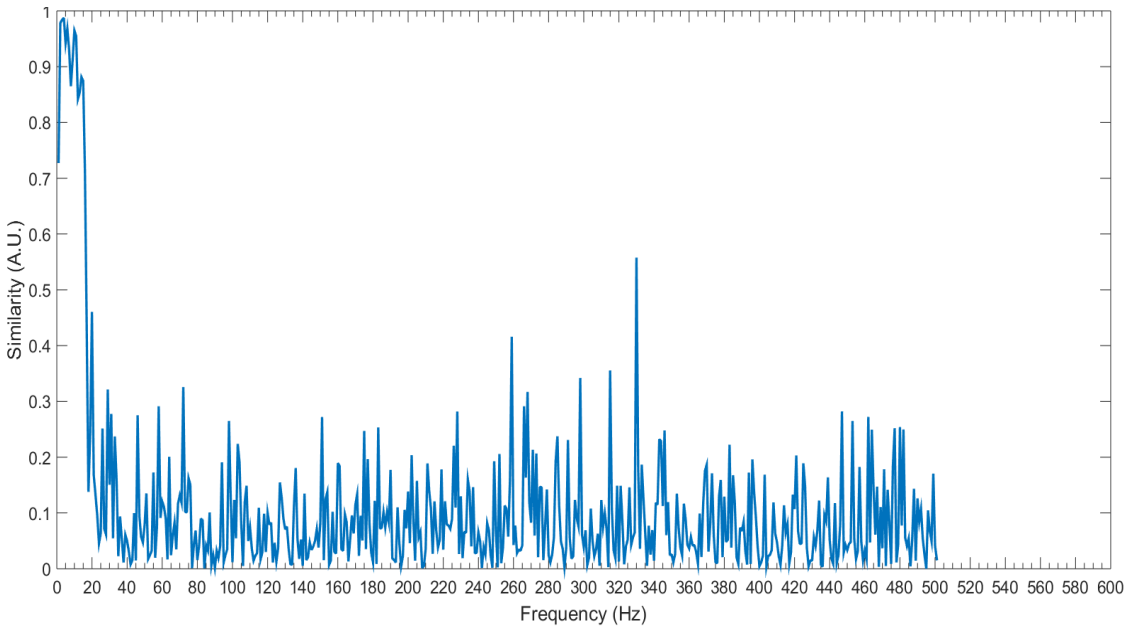

Figure 3-7 Spectral coherence

Once this couple of waveforms is defined, a search for the peaks [Figure 3-8] that correspond to the heartbeat is done and the area preceding each peak is considered for next processing.

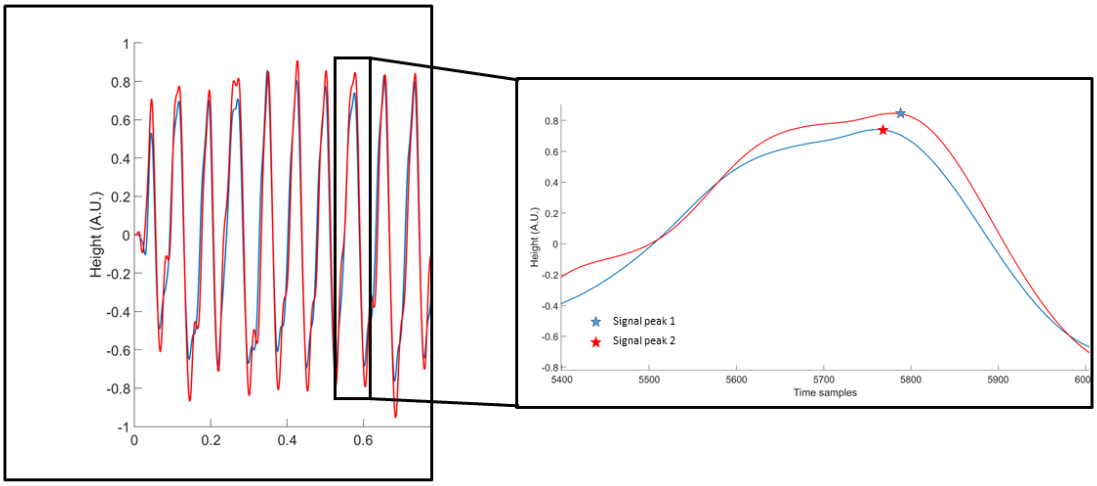

Figure 3-8 Peaks on the heartbeat waveforms

Now, for both waveforms, calculation of the second derivative is performed. The peak in the second derivative soon preceding the instant in which the peak is found in the original waveform, correspond to the "systolic foot" [79] that is the instant on which the initial phase of the heart compression starts and that constitutes a reliable time reference for the sphygmic wave [Figure 3-9]. The systolic foot is used as a reference because it is free from the effect of the reflected wave inside the artery.

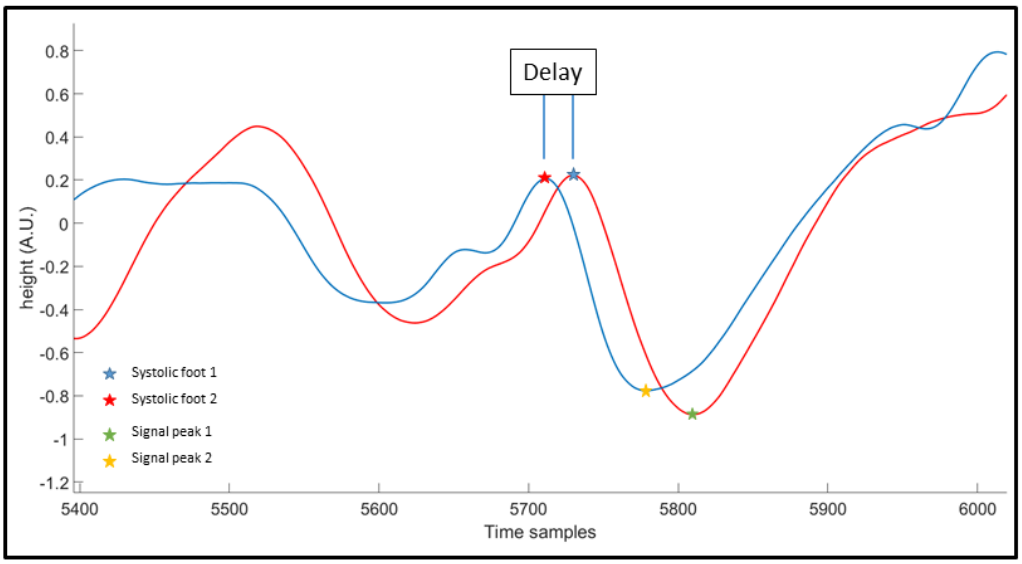

Figure 3-9 Second derivative of the original waveforms and systolic feet in reference of the pulse peaks

The time difference between two corresponding systolic feet is the time delay of the pressure wave between the two checkpoints and is what we are looking for. For each pulse a different time delay is provided, that is because of physiological signals that, by their nature, are never precise or synchronized. So, what is done now, is to collect all the delays and calculate an “average delay”, considering only the values that are in a certain range of variance thus to provide a more precise and reliable value. The delay finally obtained is then used to calculate the PWV.

c. Final Results

On this final section, I will report the results obtained by the clinical tests made during the development of this project. Some simulations were also performed on the obtained data to understand how the reliability of the measure changes by changing the quantization and the sampling frequency, so to calibrate components and therefore contain costs. All data are taken in the same conditions and on healthy volunteers with age going from 18 to 65 years, both males and females.

v. Prototype 1

The following data refers to the PWVs measured with the Prototype 1 on ten volunteers. As mentioned before, three measurements were obtained for each side of the neck, so the data corresponds to the right and left carotid of the volunteers. Because of the physical conformation of the two carotids, the blood flow is different, and so the intensity of the pulse that can be recognized. In particular, left carotid has a weaker pulse, so data is less reliable and more prone to errors and artifacts. A general graphic user interface of the acquisition panel implemented by Matlab is presented in [Figure 3-10].

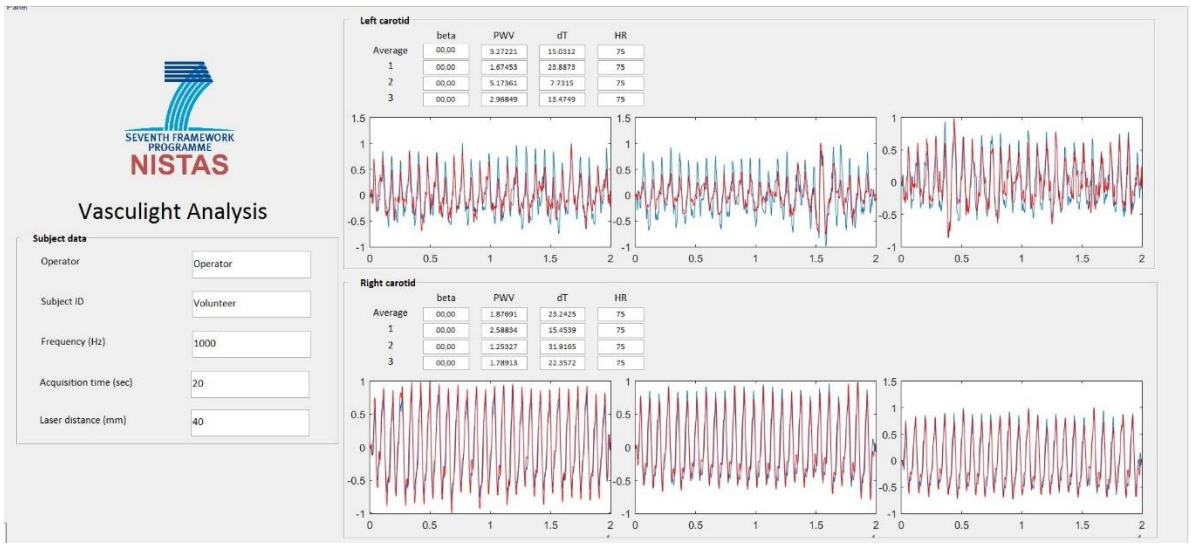

Figure 3-10 GUI panel

On the left panel, the technical and information data are reported, which are useful to calculate and organize data. The upper and lower panels, instead, show the acquired signals superposed on each graph and the calculated PWV, delay times (dT), heart rate (HR) and beta parameter. For the causes previously mentioned, it could be noticed that the left signals are more disturbed and noisy than the right signals.

For a better comparison, final data in [Table 3-1] are organized in left and right carotid that are in turn divided into three measures (rows) for each of the ten volunteer (columns). Each column reports these three measures, also provides their mean value and the standard deviation to have an idea of the repeatability of the measure.

	Vol #1	Vol #2	Vol #3	Vol #4	Vol #5	Vol #6	Vol #7	Vol #8	Vol #9	Vol #10
SX	3.62	5.35	0.96	3.56	2.61	0.95	3.99	1.96	1.30	5.17
	3.95	4.19	5.59	4.90	2.56	1.01	7.68	1.65	1.68	5.27
	3.49	4.52	5.13	4.00	2.56	1.00	5.35	1.01	1.72	4.50
mean sx	3.69	4.69	3.89	4.15	2.57	0.99	5.67	1.54	1.57	4.98
STD-SX	0.24	0.60	2.55	0.68	0.03	0.03	1.87	0.48	0.23	0.42

	Vol #1	Vol #2	Vol #3	Vol #4	Vol #5	Vol #6	Vol #7	Vol #8	Vol #9	Vol #10
DX	2.14	4.71	3.67	17.29	4.05	4.39	6.21	2.96	4.13	2.86
	1.62	4.34	4.58	24.44	3.28	4.02	24.88	2.90	3.98	2.36
	1.84	3.76	3.56	7.74	2.83	4.24	12.59	2.64	4.37	2.26
mean dx	1.87	4.27	3.94	16.49	3.39	4.21	14.56	2.84	4.16	2.49
STD-DX	0.26	0.48	0.56	8.38	0.62	0.19	9.49	0.17	0.20	0.32

Table 3-1 Final data acquired from ten volunteers

By looking at the tables above, it could be noticed that most of the measures have a low standard deviation, that means that acquired data is reliable. Higher STDs anyway, are due to some errors in the signals of which we already talked in section b, and that couldn't be recovered with my algorithm.

Figure 3-11 shows the distribution of the three measure for each volunteer to have an idea of the repeatability of the measures at a glance. At this step, we cannot define a correlation between the status of the cardiovascular system and the PWV though we have some reference values presented before in

Table 2-1. Indeed, the values in that table could differ from the ones we measured because of the different process of detection. The pressure applied by the Eco-Doppler device currently used to detect PWV could locally change the rigidity of the vessels and so alter the final result. By logic, this pressure should contribute to raising the PWV and indeed, expected values for a healthy patient are higher than the ones we found on the same kind of individual without applying pressure on the neck. This brings us to the need of defining a new golden standard that could be found when the final prototype is ready for clinical trial. What it matters now, is that we have a repeatable measure that assures that the measured values are consistent.

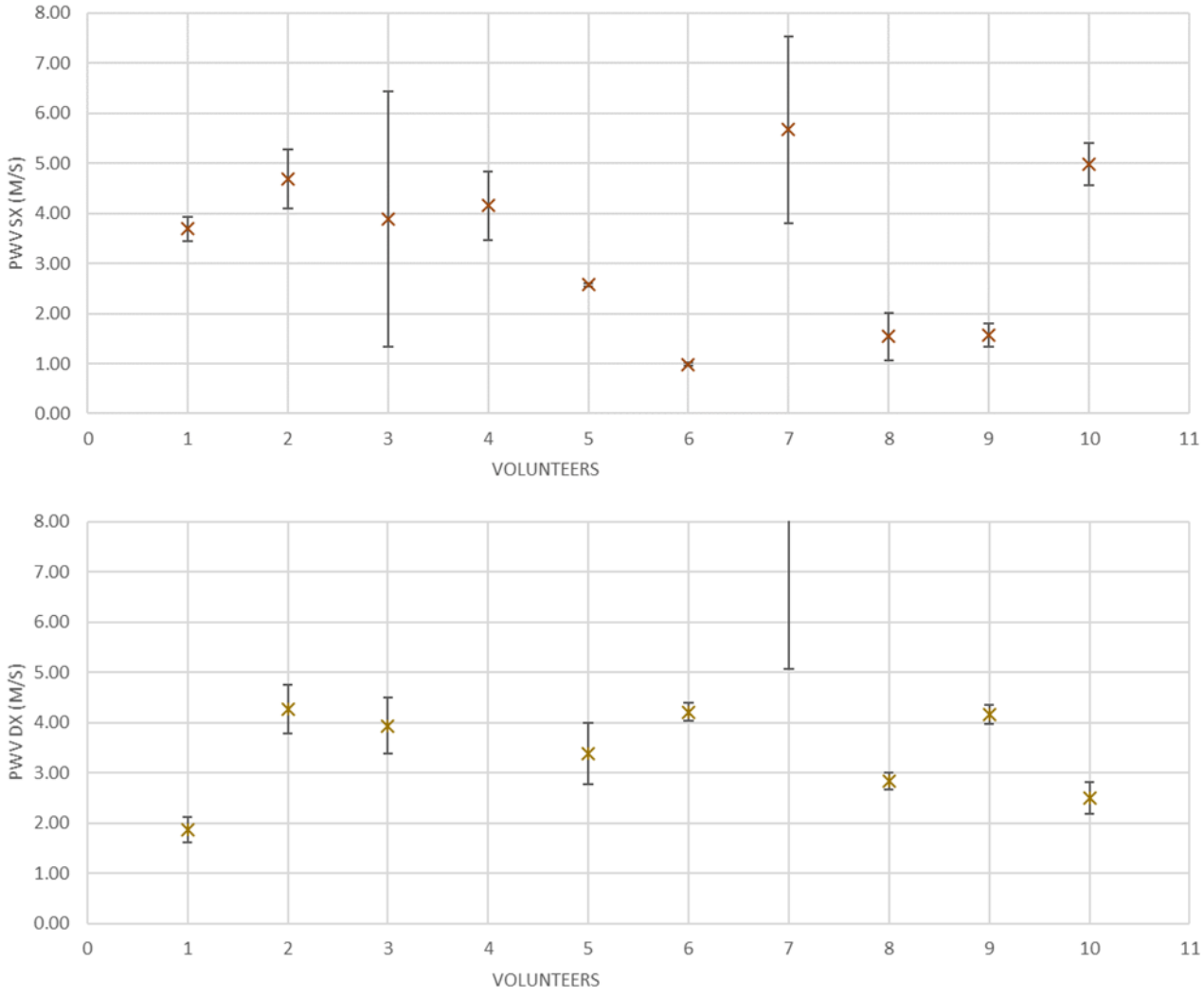

Figure 3-11 Graphics of PWV distribution for each volunteer (upper graphic refer to left side of the neck and lower graphic refer to the right side)

Resampling. To have an idea of how result changes accordingly to the sampling frequency, some resampling process was performed on available data at different sample frequency. Results of resampling of data coming from three volunteers are reported in Table 3-2 and Figure 3-12.

	Normal			Resampling (200 Hz)			Resampling (100 Hz)		
	Vol #1	Vol #2	Vol #4	Vol #1	Vol #2	Vol #4	Vol #1	Vol #2	Vol #4
SX1	3.62	5.35	3.56	3.58	2.41	2.40	3.62	0.59	1.29
SX2	3.95	4.19	4.90	3.58	0.88	1.12	3.81	0.96	3.28
SX3	3.49	4.52	4.00	3.36	2.14	1.92	3.54	1.91	2.87
STD SX	0.24	0.60	0.68	0.13	0.82	0.64	0.14	0.68	1.05
DX1	2.14	4.71	17.29	2.20	4.14	1.76	1.99	3.60	13.04
DX2	1.62	4.34	24.44	1.59	3.90	1.90	1.48	3.56	20.94
DX3	1.84	3.76	7.74	1.82	3.08	2.60	1.79	2.55	12.67
STD DX	0.26	0.48	8.38	0.31	0.56	0.45	0.26	0.60	4.67
VAR-SX	6.45	12.71	16.44	3.63	45.15	35.48	3.72	58.97	42.33
VAR-DX	14.00	11.28	50.81	16.36	15.10	21.67	14.70	18.48	30.04

Table 3-2 Resampling table

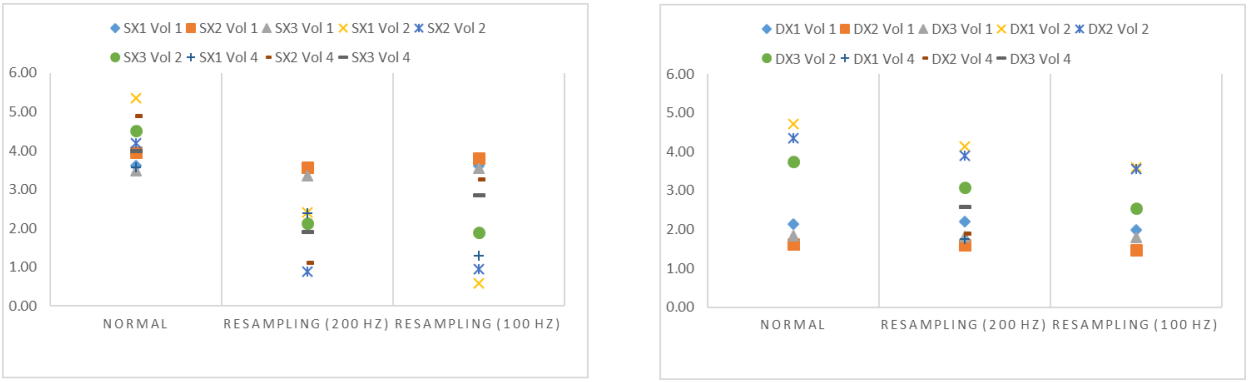

Figure 3-12 Resampling graph

From the data obtained, it could be noticed that the sub-sampling brings to a degradation of the signals that induces errors on the delay evaluation. As the time interval becomes higher, the final PWV instead becomes lower up to 1 m/s for every 100 Hz of subsampling. Furthermore, the degradation of the signals turns out to be less influent for signals with a lower standard deviation, pointing out the robustness of the measure.

Re-quantization. On the heels of the previous resampling, it was also worth to evaluate the effects of the re-quantization of the signals. Here we considered four steps of re-quantization intervals performed on three different sets of data from the same number of volunteers. Results are presented in Table 3-3 and Figure 3-13.

	Normal			Req. (5 um)			Req. (10 um)			Req. (20 um)			Req. (40 um)		
	Vol #1	Vol #2	Vol #11	Vol #1	Vol #2	Vol #11	Vol #1	Vol #2	Vol #11	Vol #1	Vol #2	Vol #11	Vol #1	Vol #2	Vol #11
SX1	3.62	2.75	4.86	3.58	1.42	1.00	3.62	1.42	1.05	5.87	5.26	1.08	6.78	4.21	1.11
SX2	3.95	4.69	0.95	3.58	5.85	14.78	3.81	10.02	10.26	3.09	4.95	6.53	4.12	4.77	6.57
SX3	3.49	6.21	3.77	3.36	6.07	4.11	3.54	6.15	4.14	3.93	3.36	4.26	3.58	4.60	4.02
STD SX	0.24	1.73	2.02	0.13	2.62	7.23	0.14	4.31	4.69	1.43	1.02	2.74	1.72	0.29	2.73
DX1	2.14	4.16	7.48	2.20	4.05	9.54	1.99	4.01	5.73	2.13	4.08	5.40	1.86	3.89	9.65
DX2	1.62	3.96	6.40	1.59	5.30	9.66	1.48	4.11	7.39	1.56	4.58	26.69	1.37	3.66	3.87
DX3	1.84	3.92	6.42	1.82	3.93	7.06	1.79	3.88	6.51	1.79	3.57	6.67	1.83	3.03	5.09
STD DX	0.26	0.13	0.62	0.31	0.76	1.47	0.26	0.12	0.83	0.29	0.50	11.94	0.27	0.44	3.05

Table 3-3 Re-quantization table

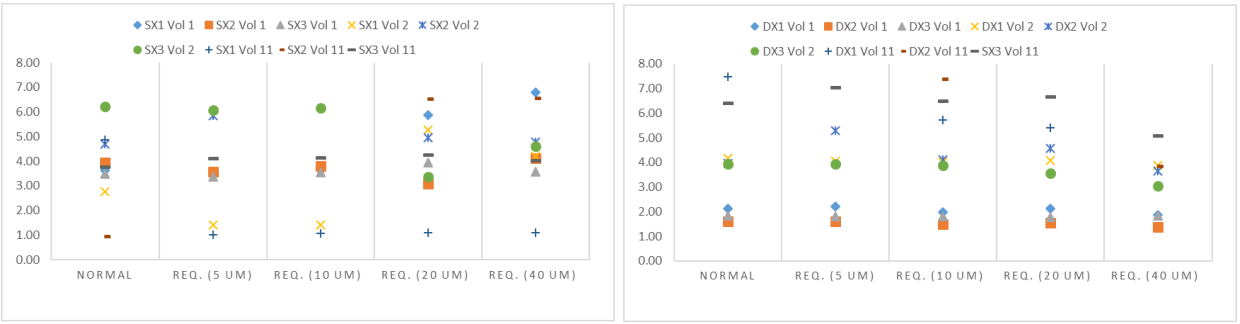

Figure 3-13 Re-quantization graph

The process of re-quantization does not bring important negative effect until it is kept under 10 µm, but it is heavy once this limit is crossed. Like resampling, the effects are more evident on signals with high standard deviation.

vi. Prototype 2

The construction of the new prototype needed a complete adaptation of the algorithm to the new components. This is necessary because we are now using a different hardware with which we can manage directly the image of the sensor and the LED sources. For that reason, a standalone software tailored on these components was built by our partner. Furthermore, this software was designed to provide a clear interface for the operator and a set of instruments needed to store data and parameters of patients. An example of what the GUI looks like is showed in Figure 3-14.

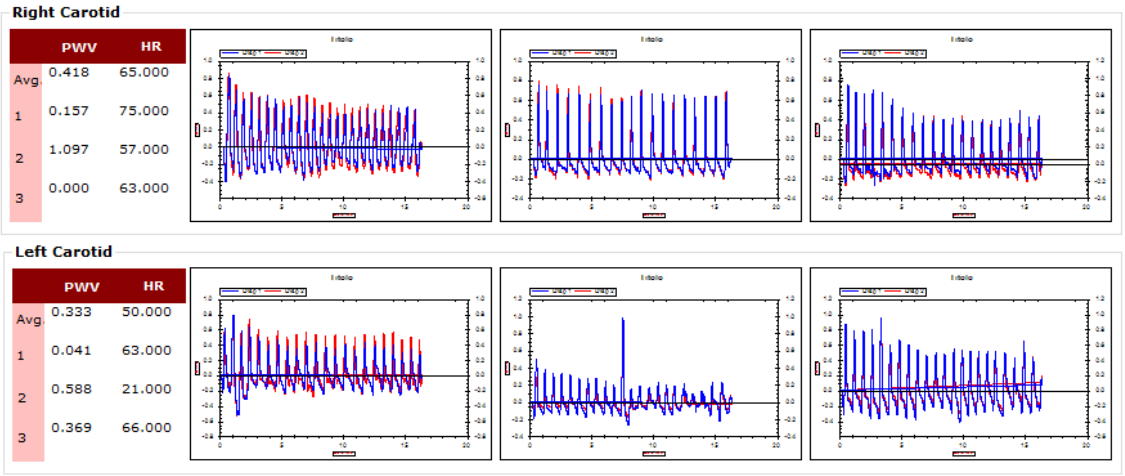

Figure 3-14 GUI interface of Prototype 2 (data on the left are just for the sake of an example)

Like the previous software, on the upper and lower panels are showed the acquired signals superposed on the same graph.

Currently, some clinical trials are still under execution by our medical partner "Policlinico San Matteo" in Pavia. Therefore we have no available data to present in this section but, as the GUI above can suggest, they reported that realistic detection could be obtained even with this device.

4. Conclusions

As aforementioned, there is a lack of a fast screening device that could help in preventing or early recognize cardiovascular risks by local assessment of PWV without need of high specialization of the operator or time-consuming procedure. This, and the economic payoff that the spreading of this kind of device could bring, were the motivation that brought to the definition of the NISTAS project to which this thesis is dedicated. Vasculight, or rather the device produced at the end of the project, is a non-invasive and contactless device that, by exploiting light sources like LEDs and light sensors like CCD, could detect the Pulse Wave Velocity (PWV), which is the speed of the pressure wave of the blood traveling in arteries. This PWV is related to the arterial stiffness that is in turn related to most of the cardiovascular diseases. Indeed, the elasticity of the vessels change with aging and with the presence of CVD causes like arteriosclerosis so, the response of the walls at the passage of the pressure wave, is relative to this elasticity and lead to high PWV when the vessel is rigid.

Vasculight is a device designed to be cost-effective, easy and ready to use and to be deployed in many hospitals and points of care by taking advantage of the PWV measurement in helping with CVD prevention and monitoring, and contribute in decreasing welfare costs.

The technology behind it is based on laser triangulation, a well-known technique employed to detect vibration and small movements of the surfaces. This technology is the basis in which lays the simple idea that gave birth to the NISTAS project. By detecting the pulse wave with two triangulators spaced by a known distance and recording the time needed by the wave to cross both the checkpoints, we can easily calculate the speed of the traveling blood flow that is the PWV we are looking for.

In this project, many industrial and clinical parties were involved, each one giving its contribution in building or testing the device. In particular, I worked closely with the “Centre of genetic and cardiovascular disease” of the “IRCSS Policlinico San Matteo foundation” in Pavia that contributed with both their medical knowledge and their clinical support during the testing phases of both prototypes. Furthermore, I also worked in strict collaboration with “Saphyrion Sagl” where I contributed to the development of the final software that drives the prototype 2 and “Julight S.R.L.” that provided their technical knowledge and support in optometry.

The aim of my work of thesis was so to find efficient solutions to perform the PWV detection and to address the issues so that they could be implemented in the final prototype which was the purpose of the NISTAS project.

I succeeded in that by first building and configure the preliminary prototype with commercial components to perform test and experiment useful to define the requirements of the final prototype. By mean of the preliminary prototype, I defined a clinical procedure to acquire data from the volunteers and to test the device during its development. Data was required as a basis to design the algorithm that manages the signal acquisition and processing. Later, I identified a technique that was proved to be effective in extrapolating the most significant information out of the tridimensional raw data coming from the two sensors by comparing them in the frequency domain. Once I obtained two signals corresponding to the pressure pulses acquired from the two sensors, I defined a technique to recover noisy and incomplete data and to calculate the delay between both so then I can calculate the PWV. Results and problems find out on this phase, were useful to define the advantages and limits of the techniques I used and to design the final prototype and its operation. Indeed, it is currently working and in use at the “Policlinico San Matteo” for further analysis.

Finally, as we saw in the final chapter, the results that I obtained are encouraging because they show that consecutive measures with small errors can be performed on the same patient. Moreover, despite mean values showed in Figure 3-11 are lower than we expected, they

oscillate around the same values as could be more evinced from the measures of the right carotid. I found out that it depends on the different kind of technique used to detect PWV as already explained.

Further work is currently in execution by our medical partner that is performing clinical trials to find a new Gold Standard for this device as needed by the different and innovative technique that we are using.

Bibliography

[1] World Healt Organization WHO, «Global Health Observatory data repository,» [Online]. Available: http://apps.who.int/gho/data/node.main.PROJNUMWORLD?lang=en.

[2] D. E. Bloom, C. Elizabeth T. e J.-L. Eva, The Global Economic Burden of Non-communicable Diseases, World Economic Forum, 2011.

[3] World Healt Organization WHO, «World Health Statistics 2014,» [Online]. Available: http://www.who.int/gho/publications/world_health_statistics/2014/en/.

[4] H. Bolooki, «acute myocardial infarction,» in *CURRENT CLINICAL MEDICINE*, Saunders, 2009.

[5] OECD - OCSE, «Health Care Quality Indicators - Acute Care,» [Online]. Available: http://www.oecd.org/els/health-systems/hcqi-acute-care.htm.

[6] World Healt Organization WHO, «Global Health Observatory (GHO) data,» [Online]. Available: http://www.who.int/gho/mortality_burden_disease/en/.

[7] R. L. Sacco, S. E. Kasner, J. P. Broderick e et al., «An Updated Definition of Stroke for the 21st Century,» *Stroke,* vol. 44, n. 7, July 2013.

[8] E. C. Jauch, «Ischemic Stroke,» 7 2016. [Online]. Available: http://emedicine.medscape.com/article/1916852-overview.

[9] D. F. Hanley, «Hemorrhagic Stroke: Introduction,» *Stroke,* vol. 44, n. 6 suppl 1, 2013.

[10] J. D. Easton, «Definition and Evaluation of Transient Ischemic Attack,» *Stroke,* vol. 40, n. 6, 2009.

[11] M. H. Drazner, «The Progression of Hypertensive Heart Disease,» *Circulation,* vol. 123, n. 3, 2011.

[12] S. S. Mahmood, D. Levy, R. S. Vasan e T. J. Wangb, «The Framingham Heart Study and the Epidemiology of Cardiovascular Diseases: A Historical Perspective,» *The Lancet,* vol. 383, n. 9924, pp. 999-1008, 2004.

[13] J. H. Choudhury, «Modifiable and Non-Modifiable Risk Factors of Stroke: A Review Update,» *Journal of National Institute of Neurosciences Bangladesh,* vol. 1, n. 1, 2015.

[14] R. Ibekwe, «Modifiable Risk factors of Hypertension and Socio-demographic Profile in Oghara, Delta State; Prevalence and Correlates,» *Annals of Medical and Health Sciences Research,* vol. 5, n. 1, pp. 71-77, 2015.

[15] R. Twombly, «Tobacco Use a Leading Global Cancer Risk, Report Says,» *Journal of the National Cancer Institute,* vol. 95, n. 1, pp. 11-12, 2003.

[16] S. Mendis, P. Puska e B. Norrving, Global Atlas on Cardiovascular Disease Prevention and Control., Geneva: World Health Organization, 2011.

[17] Services, U.S. Department of Health and Human, «The Health Benefits of Smoking Cessation,» DHHS Publication No. (CDC) 90-8416, 1990.

[18] C. S. Fox, «Cardiovascular Disease Risk Factors, Type 2 Diabetes Mellitus, and the Framingham Heart Study,» *Trends in cardiovascular medicine,* vol. 20, n. 3, pp. 90-95, 2010.

[19] International Diabetes Federation (IDF), «IDF Diabetes Atlas – Seventh Edition,» Bruxelles, 2015.

[20] B. Nordestgaard, M. Chapman, K. Ray, J. Borén, F. Andreotti, G. Watts, H. Ginsberg, P. Amarenco, A. Catapano, O. Descamps, E. Fisher, P. Kovanen, J. Kuivenhoven, P. Lesnik, L.

Masana, Z. Reiner, M. Taskinen, L. Tokgözoglu e Tybjærg, «Lipoprotein(a) as a cardiovascular risk factor: current status,» *European Heart Journal,* n. 31, p. 2844–2853, December 2010.

[21] A. L. Chandrashekhar Y, «Exercise as a coronary protective factor,» *American heart journal,* n. 122, pp. 1723-1739, 1991.

[22] P. W. Siri-Tarino, «Saturated fat, carbohydrate, and cardiovascular disease,» *The American Journal of Clinical Nutrition,* vol. 91, n. 3, pp. 502-509, 2010.

[23] R. Dhingra, «Age as a Cardiovascular Risk Factor,» *The Medical Clinics of North America,* vol. 96, n. 1, pp. 87-91, 2012.

[24] A. Maas e Y. Appelman, «Gender differences in coronary heart disease,» *netherland hearth journal,* vol. 18, n. 12, pp. 598-602, 2010.

[25] M. R. Kolber, «Family history of cardiovascular disease,» *Canadian Family Physician,* vol. 60, n. 11, 2014.

[26] P. Puska, E. Vartiainen, J. Tuomilehto, V. Salomaa e A. Nissinen, «Changes in premature deaths in Finland: successful long-term prevention of cardiovascular diseases,» *Bullettin of World Health Organization,* vol. 76, n. 4, pp. 419-425, 1998.

[27] Beaglehole, «International trends in coronary heart disease mortality and incidence rates.,» *Journal of Cardiovascular risk,* vol. 6, n. 2, 1999.

[28] Hardoon, «How Much of the Recent Decline in the Incidence of Myocardial Infarction in British Men Can Be Explained by Changes in Cardiovascular Risk Factors?,» *Circulation,* vol. 117, n. 5, 2008.

[29] Mirzaei, «Coronary heart disease epidemics: not all the same.,» *Hearth,* vol. 95, n. 9, 2009.

[30] Unal, «Explaining the decline in coronary heart disease mortality in England and Wales between 1981 and 2000.,» *Circulation,* vol. 109, n. 9, 2004.

[31] Omran, «The epidemiologic transition. A theory of the epidemiology of population change.,» *The Milbank Quarterly,* vol. 49, n. 4, 1971.

[32] G. e. al, Disease control priorities in developing countries., New York: Oxford University Press, 2006.

[33] Ezzati, «Rethinking the "Diseases of Affluence" Paradigm: Global Patterns of Nutritional Risks in Relation to Economic Development,» *PLOS Medicine,* vol. 2, n. 5, 2005.

[34] Gaziano, «Cost of treating non-optimal blood pressure in select low and middle income countries in comparison to the United States,» in *Background paper commissioned by the Committee on Preventing the Global Epidemic of Cardiovascular Disease*, 2009.

[35] L.-J. e. al, «Heart disease and stroke statistics--2009 update: a report from the American Heart Association Statistics Committee and Stroke Statistics Subcommittee.,» *Circulation,* vol. 119, n. 3, 2009.

[36] Pestana, Steyn, Leiman e Hartzenberg, «The direct and indirect costs of cardiovascular disease in South Africa in 1991.,» *South African Medical Journal,* vol. 86, n. 6, 1996.

[37] World Healt Organization WHO, The World Health Report, World Healt Organization WHO, 2005a.

[38] E. Briones, J. Lacalle, I. Marin-Leon e J. Rueda, «Transmyocardial laser revascularization versus medical therapy for refractory angina,» *Cochrane Database Syst Rev,* 2015.

[39] B. Lauer, U. Junghans, F. Stahl, R. Kluge, S. N. Oesterle e G. Schuler, «Catheter-based percutaneous myocardial laser revascularization in patients with end-stage coronary artery disease,» *Journal of the American College of Cardiology,* vol. 34, n. 6, p. 1663–1670, 1999.

[40] J. van der Sloot, M. Huikeshoven, R. Tukkie e e. al., «Transmyocardial revascularization using an XeCl excimer laser: results of a randomized trial.,» *The Annals of thoracic surgery,* vol. 78, n. 3, 2004.

[41] S. K. Estvold, F. Mordini, Y. Zhou, Z. X. Yu, V. Sachdev, A. Arai e K. A. Horvath, «Does Laser Type Impact Myocardial Function Following Transmyocardial Laser Revascularization?,» *Lasers in Surgery and Medicine,* vol. 42, n. 10, pp. 906-911, 2010.

[42] P. Fisher, T. Khomoto, C. DeRosa, H. Spotnitz, C. Smith e D. Burkhoff, «Histologic analysis of transmyocardial channels: comparison of CO2 and holmium:YAG lasers,» *Ann Thorac Surg,* vol. 64, n. 2, pp. 466-72, 1997.

[43] K. Horvath, «Thoracoscopic Transmyocardial Laser Revascularization,» *Operative Techniques in Thoracic and Cardiovascular Surgery,* vol. 6, n. 3, pp. 132-139, 2001.

[44] « Percutaneous transmyocardial laser revascularization: an overview,» *Cathet Cardiovasc Interven,* vol. 47, pp. 354-59, 1999.

[45] M. Saririan e M. J. Eisenberg, «Myocardial Laser Revascularization for the Treatment of End-Stage Coronary Artery Disease,» *Journal of the American College of Cardiology,* vol. 41, n. 2, pp. 173-183, 2003.

[46] N. Gassler, H. Wintzer, H. Stubbe, A. Wullbrand e U. Helmchen, «Transmyocardial laser revascularization. Histological features in human nonresponder myocardium.,» *Circulation,* vol. 95, n. 2, pp. 371-5, 1997.

[47] T. Sundt e K. Kwong, «Clinical experience with the holmium:YAG laser for transmyocardial laser revascularization and myocardial denervation as a mechanism.,» *Seminars in thoracic and cardiovasular surgery,* vol. 11, n. 1, pp. 19-23, 1999.

[48] I. Wolf-de Jonge, J. Beek e R. Balm, «25 years of laser assisted vascular anastomosis (LAVA): what have we learned?,» *European Journal of Vascular and Endovascular Surgery,* vol. 27, n. 5, pp. 466-476, 2004.

[49] W. J. McCarthy, R. S. Hartz, J. S. T. Yao, V. S. Sottiurai, H. C. Kwaan e L. L. Michaelis, «Vascular anastomoses with laser energy,» *Journal of Vascular Surgery,* vol. 3, n. 1, pp. 32-41, 1986.

[50] K. McNally, S. BS, N. Bhavaraju, M. Ducros, A. Welch e D. JM, «Optical and thermal characterization of albumin protein solders,» *Applied Optics,* vol. 38, pp. 6661-6672, 1999.

[51] D. Huang, «Optical Coherence Tomography,» *Science,* vol. 254, n. 5035, pp. 1178-1181, 1991.

[52] G. Guagliumi e V. Sirbu, «Optical coherence tomography: high resolution intravascular imaging to evaluate vascular healing after coronary stenting,» *Catheter Cardiovasc Interv,* vol. 72, pp. 237-247, 2008.

[53] M. Choma, M. Sarunic, C. Yang e J. Izatt, «Sensitivity advantage of swept source and Fourier domain optical coherence tomography.,» *Optical Express,* vol. 11, pp. 2183-9, 2003.

[54] T. Roleder e W. Wojakowski, «Intravascular ultrasound, optical coherence tomography and near infrared spectroscopy,» *Imaging in Coronary Artery Disease,* vol. 57, n. 6, pp. 439-445, 2015.

[55] J. D. Caplan e a. et, «Near-Infrared Spectroscopy for the Detection of Vulnerable Coronary Artery Plaques,» *Journal of the American College of Cardiology,* vol. 47, n. 8, 2006.

[56] P. Geladi, «Chemometrics in spectroscopy. Part 1. Classical chemometrics,» *Spectrochimica Acta Part B,* vol. 58, pp. 767-782, 2003.

[57] «A TCT Breakfast Symposium Summary: Imaging STEMI Culprit Plaques with Near-Infrared Spectroscopy,» [Online]. Available: http://www.cathlabdigest.com/articles/TCT-Breakfast-Symposium-Summary-Imaging-STEMI-Culprit-Plaques-Near-Infrared-Spectroscopy.

[58] A. Fard, P. Vacas-Jacques, E. Hamidi, H. Wang, R. Carruth, J. Gardecki e G. Tearney, «Optical coherence tomography--near infrared spectroscopy system and catheter for intravascular imaging,» *Optical Express,* vol. 21, n. 25, 2013.

[59] I. Clausen e T. Glott, «Development of clinically relevant implantable pressure sensors: perspectives and challenges.,» *Sensors,* vol. 14, n. 9, pp. 17686-702, 2014.

[60] «MTI instruments,» [Online]. Available: http://www.mtiinstruments.com/products/fiberopticmeasurement.aspx.

[61] W. L. Knute, «Fiber optic measurement system having a reference conductor for controlling the energy level of the light source». US Brevetto US5065010 A, 12 november 1991.

[62] É. Pinet, «Fabry-Pérot Fiber-Optic Sensors for Physical Parameters Measurement in Challenging Conditions,» *Journal of Sensors,* vol. 2009, n. 2009, 2009.

[63] «sensorland,» [Online]. Available: http://www.sensorland.com/HowPage072.html.

[64] É. Pinet, E. Cibul e D. Donlagic, «Ultra-miniature all-glass Fabry-Pérot pressure sensor,» *Fiber Optic Sensors and Applications V,* 2007.

[65] C. Palombo e M. Kozakova, «Arterial stiffness, atherosclerosis and cardiovascular risk: Pathophysiologic mechanisms and emerging clinical indications,» *Vascul Pharmacol.,* vol. 77, pp. 1-7, 2016.

[66] S. Laurent, J. Cockcroft, L. V. Bortel, P. Boutouyrie, C. Giannattasio, D. Hayoz, B. Pannier, C. Vlachopoulos, I. Wilkinson, H. Struijker e Boudier, «Expert consensus document on arterial stiffness: methodological issues and clinical applications,» *Eur Heart Journal,* vol. 27, pp. 2588-2605, 2006.

[67] C. Liakos, C. Grassos e D. Babalis, «ESH/ESC guidelines for the management of arterial hypertension: what has changed in daily clinical practice?,» *High Blood Press Cardiovasc Prev.,* vol. 22, pp. 43-53, 2015.

[68] T. Pereira, C. Correia e J. Cardoso, «Novel Methods for Pulse Wave Velocity Measurement,» *Med Biol Eng.,* vol. 35, pp. 555-565, 2015.

[69] [Online]. Available: www.olympus.com.ru/medical/en/medical_systems/products_services/product_details/product_details_5824.jsp.

[70] «Pulsepen,» [Online]. Available: http://pulsepen.com/pulsepen.html.

[71] «Complior,» [Online]. Available: http://www.complior.com/products.

[72] «SphygmoCor,» [Online]. Available: http://atcormedical.com/.

[73] «European Heart Journal,» vol. 31, p. 2338–2350, 2010.

[74] M. Instruments, «Laser Triangulation System,» [Online]. Available: http://www.mtiinstruments.com/products/lasertriangulation.aspx.

[75] P. T. M. G. I. G. N. M. B. G. D. F. M. V. J. Calabia, «Doppler ultrasound in the measurement of pulse wave velocity: agreement with the Complior method,» *Cardiovascular Ultrasound,* vol. 9, 2011.

[76] T. T. e. al, «Measurement of pulse wave velocity: site matters.,» *Journal of Hypertension,* vol. 25, n. 2, 2007.

[77] «LJ-V7080 Sensor Head,» [Online]. Available: http://www.keyence.eu/products/measure/laser-2d/lj-v/models/lj-v7080/index.jsp.

[78] «Spectral Coherence,» [Online]. Available: https://en.wikipedia.org/wiki/Coherence_(signal_processing).

[79] E. Hermeling, K. Reesink, R. Reneman e A. Hoeks, «Confluence of incident and reflected waves interferes with systolic foot detection of the carotid artery distension waveform,» *Journal of hypertension,* vol. 26, pp. 2374-2380, 2008.

[80] G. Giuliani, M. Norgia, S. Donati e T. Bosch, «Laser diode self-mixing technique for sensing applications,» *Journal of Optics A: Pure and Applied Optics,* vol. 4, n. 6, pp. S283-S294, 2002.

[81] F. F. M. Mul, M. H. Koelink e A. L. Weijers, «Self-mixing laser-Doppler velocimetry of liquid flow and of blood perfusion in tissue,» *Applied optics,* vol. 31, n. 27, p. 5844–5851, 1992.

[82] K. Meigas, H. Hinrikus, R. Kattai e J. Lass, «Self-mixing in a diode laser as a method for cardiovascular diagnostics as a method for cardiovascular diagnostics,» *Journal of Biomedic optics,* vol. 8, n. 1, pp. 152-60, 2003.

[83] K. C. d. Sousa, A. C. Domingues, P. P. d. S. Pereira, S. H. Carneiro, M. V. G. d. Morais e A. T. Fabro, «Modal parameter determination of a lightweight aerospace panel using laser Doppler vibrometer measurements,» in *proceedings of the 12th international a.i.ve.la. conference on vibration measurements by laser and noncontact techniques: advances and applications*, Ancona, 2016.

[84] O. PA, «Laser-Doppler flowmetry,» *Critical review In biomediacl engineering,* vol. 18, n. 2, pp. 125-63, 1990.

[85] Y. Vlasov e S. McNab, «Losses in single-mode silicon-on-insulator strip waveguides and bends,» *Optical Express,* vol. 12, n. 8, pp. 1622-1631, 2004.

[86] M. Gnan, S. Thorns, D. S. Macintyre, R. M. D. L. Rue e M. Sorel, «Fabrication of low-loss photonic wires in silicon-on-insulator using hydrogen silsesquioxane electron- beam resist,» *Electronic Letters,* vol. 44, n. 2, pp. 115-116, 2008.

[87] M. P. Nezhad, O. Bondarenko, M. Khajavikhan, A. Simic e Y. Fainman, «Etch-free low loss silicon waveguides using hydrogen silsesquioxane oxidation masks,» *Optical express,* vol. 19, n. 20, pp. 18827-18832, 2011.

[88] F. A. Kish, D. Welch, R. Nagarajan, J. L. Pleumeekers, V. Lal, M. Ziari, A. Nilsson, M. Kato, S. Murthy, P. Evans, S. W. Corzine, M.Mitchell, P. Samra, M.Missey, S. DeMars, R. P. S. Jr, M. S. Reffle, T. Butrie, J. T. Rahn, M. V. Leeuwen e J. W. St, «Current status of large-scale InP photonic integrated circuits,» *IEEE J. Quantum Electron,* vol. 17, n. 6, pp. 1470-1489, 2011.

[89] G. Voirin, D. Gehriger, O. M. Parriaux e B. A. Usievich, «Si3N4/SiO2/Si waveguide grating for fluorescent biosensors,» *Integrated Optics Devices III,* 1999.

[90] Q. Liu, X. Tu, K. W. Kim, J. S. Kee, Y. Shin, K. Han, Y.-J. Yoon, G.-Q. Lo e M. K. Park, «Highly sensitive Mach–Zehnder interferometer biosensor based on silicon nitride slot waveguide,» *Sensors and Actuators B: Chemical,* vol. 188, pp. 681-688, 2013.

[91] Y. Li, *Miniaturized Laser Doppler Vibrometer,* Gent: Universiteit Gent, 2013.

[92] M. Bachmann, P. A. Besse e H. Melchior, «General self-imaging properties in NxN multimode interference couplers including phase relations,» *Applied Optics,* vol. 33, n. 18, 1994.

[93] Y. Li e R. Baets, «Homodyne laser Doppler vibrometer on silicon-on-insulator with integrated 90 degree optical hybrids,» *Optics Express,* vol. 21, n. 11, p. 13342, 2013.